Role of Muscle-Specific Nuclear Envelope Transmembrane Protein NET39 in Myogenic Genome Organization

A thesis submitted towards partial fulfillment of

BS-MS Dual Degree Programme by

Muhunden Nallappa Jayakrishnan

20151106

IISER Pune

Project Supervisor

Prof. Eric Schirmer

Institute of Cell Biology

The University of Edinburgh, UK

Certificate

This is to certify that this dissertation entitled "**Role of Muscle-Specific Nuclear Envelope Transmembrane Protein NET39 in Myogenic Genome Organization**" towards the partial fulfilment of the BS-MS Dual Degree programme at the Indian Institute of Science Education and Research, Pune represents original work carried out by Muhunden Nallappa Jayakrishnan at the Institute for Cell Biology, University of Edinburgh under the supervision of Prof. Eric Schirmer, Professor of Nuclear Envelope Biology, University of Edinburgh, Edinburgh during the academic year 2019-2020.

Prof. Eric Schirmer
Professor of Nuclear Envelope Biology
Institute of Cell Biology
The University of Edinburgh
Edinburgh

Muhunden Nallappa Jayakrishnan
BS-MS Student
20151106
IISER Pune

Date: 20th March 2020

Declaration

I hereby declare that the matter embodied in the report entitled "**Role of Muscle-Specific Nuclear Envelope Transmembrane Protein NET39 in Myogenic Genome Organization**" are the results of the investigations carried out by me at the Institute of Cell Biology, The University of Edinburgh, UK, under the supervision of Prof. Eric Schirmer and the same has not been submitted elsewhere for any other degree.

Prof. Eric Schirmer
Professor of Nuclear Envelope Biology
Institute of Cell Biology
The University of Edinburgh
Edinburgh

Muhunden Nallappa Jayakrishnan
BS-MS Student
20151106
IISER Pune

Date: 20th March 2020

Abstract

Studies over the past decade have shown the importance of the nuclear envelope (NE) in regulating genome organization. However, the mechanisms by which different NE components regulate genome organization through space and time in a tissue- specific manner are not completely understood. We utilized the in-vitro C2C12 myogenesis system to study local and genome wide changes in nuclear architecture during myogenesis by correlative studies of Hi-C, DamID and Microarray datasets. Our results show that the genome undergoes dynamic changes in compartmentalization and NE association. Analysis of genes under Lamina Associated Domains (LAD) and Chromatin Compartment control reveals that LADs fine tune genes expression important for myogenesis. However, dynamic changes in LADs and Chromatin Compartments do not necessarily correlate with transcriptional control. Preliminary analysis suggests that LAD functions extend beyond traditional gene regulation to possibly modulate functions of regulatory elements like ncRNA and enhancers. We then investigated potential mechanisms by which a major muscle-specific Nuclear Envelope Transmembrane Protein (NET) NET39, which is known to regulate a subset of LADs, regulates genome organization during myogenesis directly or indirectly via partner proteins identified by analysis of 'Interactome' datasets. We report that NET39 does not exert its genome organizing functions by affecting the physical features of the nucleus such as tensional forces, chromocenter organization and nuclear topology. We further show that NET39 regulates deposition of repressive histone modification H3K9Me3 on genes which get repressed during myogenesis. Finally, we also show that a subset of genes that get repressed and localize to the nuclear periphery during myogenesis get reactivated and concomitantly reposition into the nuclear interior, suggesting plasticity in myogenic genome organization. Taken together, our study gives us interesting insights into NE-genome organization interplay in myogenesis.

Index

List of Figures and Tables

Acknowledgement

Firstly, I would like to thank Prof. Eric Schirmer for providing the opportunity to explore my interests in his lab and allowing me to play around with interesting questions and techniques. Although this might have reduced my overall productivity, it allowed me to develop critical skills which have undoubtedly sculpted me into a better scientist.

I would also like to thank Charles Dixon for being a great flat mate, walking buddy and a constant source of intellectual discussions. I'm also incredibly grateful to Dr. Rafal Czapiewski, Aishwarya Sivakumar, Dr. Jose I. De Las Heras and Cristina Cardenal Peralta for helping me with various aspects of my project. I would also like to thank Dr. David Kelly and Dan Robertson from COIL for helping me with microscopy and bioinformatics respectively. I would also like to thank Dr. Kundan Sengupta (IISER Pune), Dr. Rina Rosenzweig (Weizmann Institute of Science) and Dr. Pramod Pillai (IISER Pune) for inculcating important research qualities in me during various research internships.

I also express my sincere gratitude to my friends and family who have constantly provided their support during the ups and downs of my research career. Finally, I would like to thank IISER Pune for providing incredible teaching and research facilities throughout the entire BS-MS degree.

Introduction:

Over the last few decades, studies have revealed interesting principles of how genomes are packed within the nucleus. The nucleus is highly inhomogeneous and the local microenvironment within the nucleus can greatly influence transcriptional regulation and dynamics (Kumaran et al., 2008) (Finlan et al., 2008). Chromatin can be broadly classified into euchromatin and heterochromatin, with the former generally comprising regions of active transcription while the latter refers to transcriptionally silenced regions. Genome organization within the 3D nucleus is non-random; chromosome territories and gene loci tend to occupy preferential positions within the nuclear sub volume depending on various factors like transcription factor occupancy, epigenetic status etc. (Cremer et al., 2001). In general, euchromatin tends to preferentially localize towards the nuclear interior while heterochromatin is generally found proximal to the nuclear periphery (Cremer et al., 2001) .

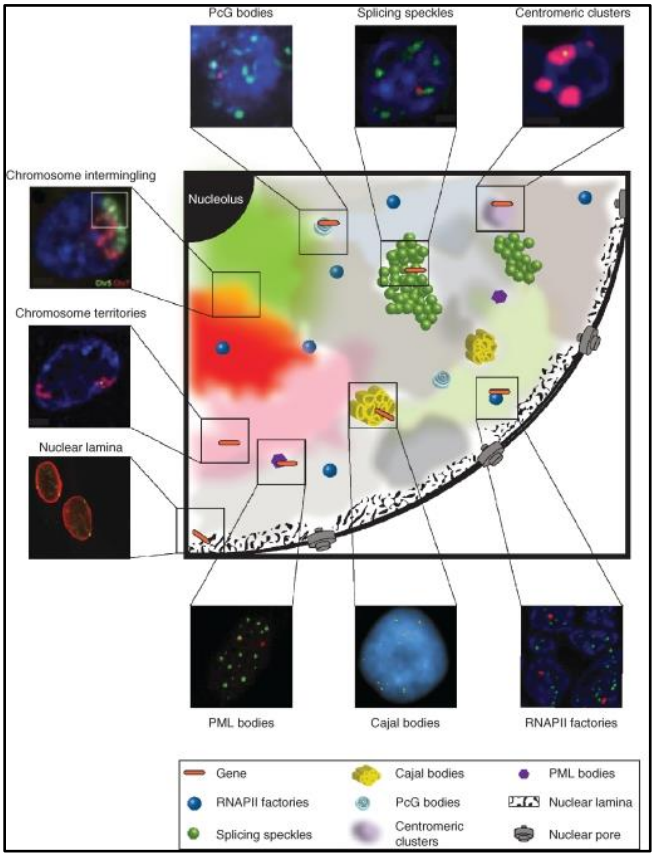

Fig 1) Schematic representing various nuclear landmarks and their spatial distribution within the 3D nucleus. Centromeric clusters and nuclear Lamina are generally associated with

transcriptionally repressive microenvironments while RNAPII factories and Speckles relate to transcriptionally permissive environments, reinforcing the idea of gene expression-spatial localization relationships. Adapted from (Ferrai et al., 2010)

However, these trends vary greatly across tissue types. Electron microscopy studies have shown that neurons tend to have lesser peripheral heterochromatin as compared to other cell types (Fawcett, 1981). Another interesting example is rod cells which show completely inverted radial distribution of euchromatin and heterochromatin (Falk et al., 2019). Further, these patterns are highly dynamic and can show active reorganization in response to external stimuli in varying timescales. For instance, heat shock responsive genes (Pradhan et al., 2020) and pluripotency regulation genes (Sivakumar et al., unpublished) show altered spatial localization when exposed to their respective stimuli in the order of minutes. On the other hand, loss of peripheral heterochromatin associated with leukocyte activation takes several days (Korfali et al., 2010) while a similar phenomenon associated with senescence takes place in a much longer timescale (Criscione et al., 2016).. However, it is important to note for these two latter phenomena that while the visual loss of dense peripheral chromatin takes days, there are many individual genes and even in the case of senescence whole chromosomes that are released from the nuclear envelope (NE) in the very short timeframes of tens of minutes to several hours (Mehta et al., 2010; Robson et al., 2017)

The NE is composed of an inner and outer nuclear membrane separated by ~50nm and is composed of a diverse group of proteins with a wide range of functions like nucleo-cytoplasmic transport, gene regulation, signal transduction and mechanical support (Hetzer, 2010). Amongst these proteins are the nuclear intermediate filaments Lamins that form a supporting meshwork beneath the NE and are involved in regulatory crosstalk across the NE through mechanosignal transduction in addition to their many other roles. The mechanistic understanding of how the NE helps in establishing genome organization patterns and the functional consequences of such patterns are topics of active research.

Chromatin associated with the NE is broadly referred to as Lamina Associated Domains (LADs). The nuclear periphery generally forms a transcriptionally repressive environment although a small subset of genes get activated at the nuclear periphery (Peric-Hupkes and van Steensel, 2010) The nuclear periphery is depleted of active histone marks like H3K4Ac and enriched for repressive histone modifications like DNA methylation, H3K27Me3, H3K9Me2 (Guelen et al., 2008) (Prokocimer et al., 2009) . Further, repressive histone modifiers like HDAC3 are present at the nuclear periphery indicating that the NE environment has proteins that can establish and maintain heterochromatin. (Demmerle et al., 2012)

No specific LAD forming complex has been defined; however, there are many different interactions that have been defined between chromatin and NE proteins that either independently summed or working interdependently likely support LAD establishment. Moreover, it is possible that these various nuclear protein interactions have different affinities contributing to LAD establishment. Lamins can directly bind and anchor chromatin via core histones (Taniura et al., 1995), although more recent studies have suggested that Lamins are not necessary for establishment of LADs (Amendola and van Steensel, 2015). Nuclear Envelope Transmembrane protein (NETs) Lap2β binds chromatin indirectly via soluble partner BAF (Furukawa et al., 2003) , but can also recruit transcription repressor cKrox to bind DNA in a sequence dependent manner (Zullo et al., 2012). Nuclear pore complex protein Nup93 may coordinate with boundary element CTCF to regulate developmentally important genes (Labade et al., 2016) while NETs like LBR interact with proteins that recognize epigenetic marks (referred to as epigenetic readers) like HP1 and MeCP2 (Ye and Worman, 1996), exploiting general heterochromatin interactions to organize chromatin at periphery. Thus, the viewpoint that the NE is an inert structural entity has been discarded in favor of the view that it has biologically active regulatory roles in organizing the genome in 3D and in spatially segregating different chromatin regions/functions.

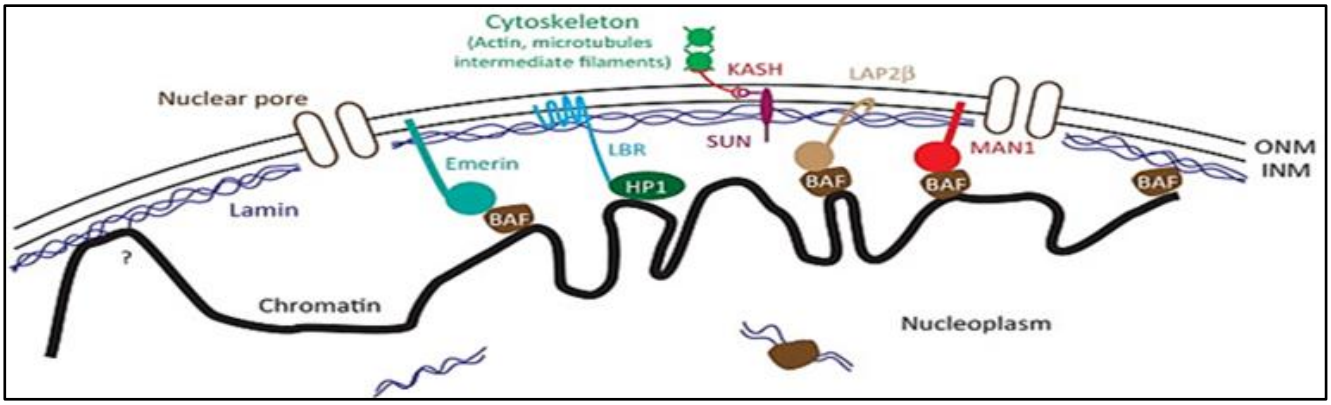

Fig 2) Schematic depicting the nuclear envelope, nuclear lamina and affinity tethering interactions among various nuclear envelope components and soluble factors that organize chromatin at the nuclear periphery. Adapted from (Towbin et al., 2013)

Commonly studied NE proteins like Lamins and Emerin are widely expressed in different kinds of tissues suggesting that they are less likely to be major drivers of tissue-specific genome organization. It is possible that these proteins might have tissue-specific interaction partners, as indicated in the previously cited example of cKrox-Lap2β tethering interaction since c-Krox is not universally expressed. However, much stronger candidates for mediating tissue-specific genome organization can be found in novel tissue-specific NE transmembrane proteins (NETs). Several studies have shown that the NE proteome is extremely diverse and only a small fraction is shared between different tissue types (Korfali et al., 2012; Schirmer et al., 2003). Several of these tissue specific NETs affect spatial regulation of genes and chromosomes and are capable of exerting their functions in heterologous systems (de Las Heras et al., 2017; Robson et al., 2016; Zuleger et al., 2013). Fat-specific NETs Tmem120A and Tmem120B were shown to be crucial for adipogenic differentiation and exert their functions by aiding establishment of fat-specific genome organization patterns (Batrakou et al., 2015), Czapiewski et al. unpub). In parallel studies, muscle specific NETs NET39, WFS1 and Tmem38a were shown to be important players in myogenic differentiation, with NET39 forming a major focus of this project (Robson et al., 2016). Mutations in most muscle-specific NETs that contribute to genome organization have now been linked to human muscle diseases (Meinke et al., 2020; Worman and Schirmer, 2015), further

underscoring the importance of tissue-specific protein chromatin interactions in development in disease.

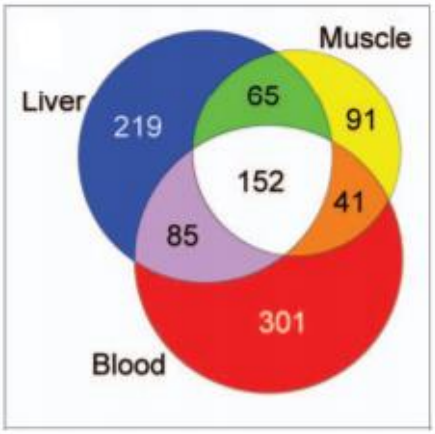

Fig 3) Venn diagram depicting the numbers of NETs overlapping between rat liver, rat muscle and human blood leukocytes expressed, highlighting diversity in NE proteome (Korfali et al)

With the advent of techniques like Chromosome Conformation Capture suite of techniques (3C, Hi-C etc.), super resolution DNA/RNA Fluorescence In Situ Hybridization (FISH) , DNA adenine methyltransferase ID (DamID) etc., coupled with great strides in sequencing and bioinformatics have allowed us to investigate spatial genome organization at an unprecedented resolution. DamID studies involve the use of a DNA Adenine Methyltransferase (DAM) module fused to a bait protein to map genomic regions interacting with the protein of interest(Greil et al., 2006). This technique has been used to provide great insights into genome-nuclear lamina interactions (Guelen et al., 2008). Hi-C, a high-throughput sequencing based method to map spatially proximal DNA-DNA contacts have revealed that the genome is partitioned into discrete Topologically Associated Domains (TADs) within which interactions are much more frequent than with other parts of the genome and often represent coordinated gene clusters (Lieberman-Aiden et al., 2009). Most TADs are developmentally conserved and loss of TAD boundaries can be pathological due to mis regulation of enhancer-gene contacts (Lupiáñez et al., 2015). Recent advances in the microscopy forefront combined with single cell Hi-C techniques have quantified cell to

cell variability and have further cemented the probabilistic nature of genome organization (Ou et al., 2017) ,(Nagano et al., 2013). With the expansion of repertoire of tools available to study genome organization, one can functionally dissect the mechanisms by which the epigenome is regulated in disease and development.

Experimental Workflow:

In this project, we aimed to develop and characterize a system which would allow us to study muscle specific patterns of genome organization. We employed the use of C2C12 in-vitro myogenesis system in which proliferating mouse myoblasts (MB) can be induced to differentiate into Myotubes (MT) by serum starvation and contact inhibition of proliferation (Fig 1)

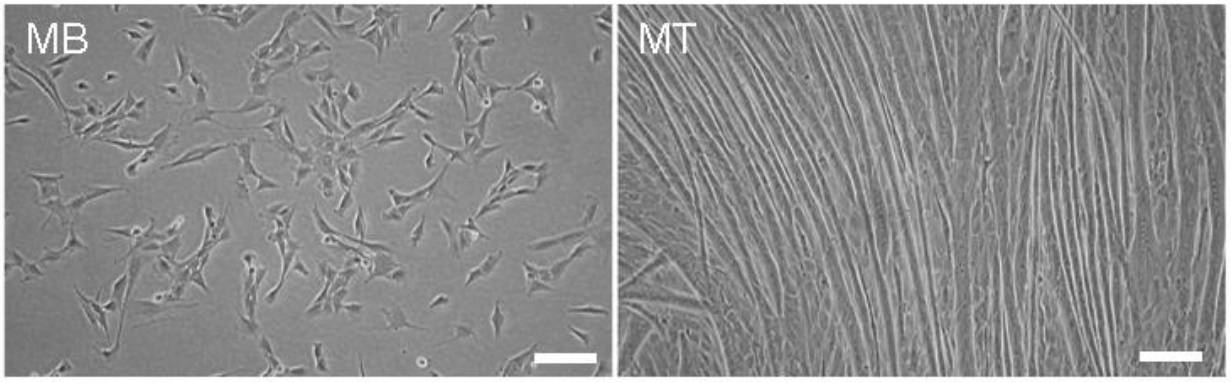

Fig 4) Phase Contrast Microscopy images of proliferating Myoblasts (MB) and 6 day differentiated Myotubes (MT). Scale bars represent 100 µm (credits: Dr. Michael Robson)

The C2C12 system is a well-established muscle differentiation system and benefits from sharing several features with the primary skeletal muscle system. Initially, we identified local and global trends between LADs, Chromatin Compartments and Transcription by performing correlative studies of DamID, Hi-C and Microarray datasets. We then analyzed the mass-spectrometry based ‘Interactome’ datasets of different NETs to understand general principles of NET mediated genome organization and potential mechanisms by which NET39 exerted its muscle genome organization effects directly or indirectly via interacting partner proteins. Specifically, we investigated if NET39 can regulate genome organization in myogenesis by i) affecting nuclear topology and chromocenter organization ii) affecting epigenetic features and iii) transcriptional control

of the LINC complex using a combination of qPCR, Imaging and ChIP approaches. Further, we also used this system to address a more general question of reprogrammability of genome organization events. For this we attempted to mimic muscle injury in vitro by treating C2C12 myotubes with a peptide toxin previously used to induce muscle injury in mice and investigating transcription and spatial positioning of three genes needed early in myogenesis, but that become repressed later in myogenesis due to the action of muscle-specific NETs.

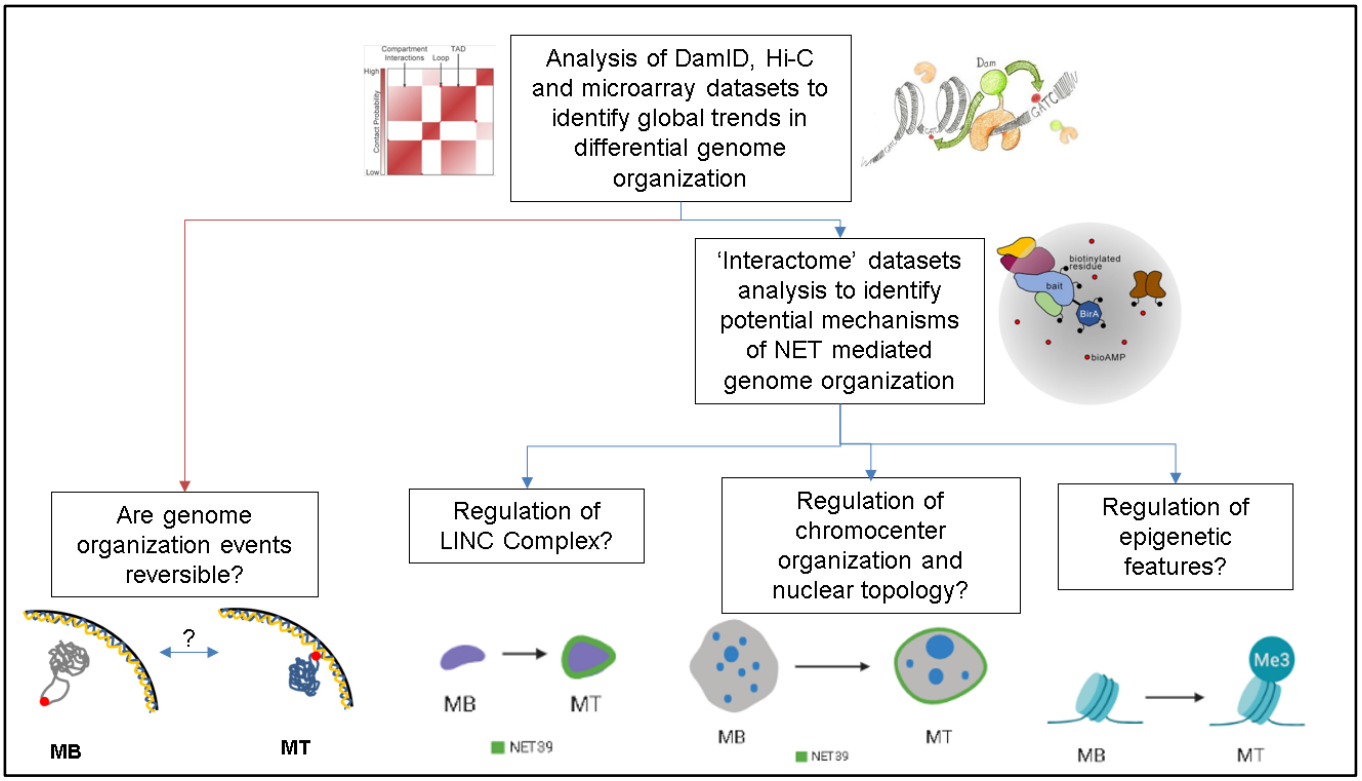

Fig 5) Schematic representing the workflow of the project. Computational studies of correlations between whole genome datasets were performed. This was followed by investigating potential mechanisms by which NET39 can exert its genome organization events. In parallel, reversibility of genome organization events during muscle injury was also investigated.

Methods:

Cell Culture: C2C12 MBs were cultured at 37°C in a humid 5% CO_2 atmosphere in DMEM supplemented with 20% FBS, 100 µg/ml streptomycin and 100 units/ml penicillin. Cells were passaged in a 1:8 dilution by trypsinization and was ensured that they do not exceed 75-80% confluency .ie. ~ 2 million cells in a 10 cm dish.

To differentiate C2C12 MBs, cells were seeded at 80-90% confluency and allowed to proliferate for 48 h before inducing differentiation by adding differentiation media (DMEM supplemented with 2% horse serum and 1% Penicillin/Streptomycin). The differentiation takes place over 6-7 days and media must be changed every 24 hours as MTs acidify the medium faster over the course of differentiation. To prevent MT contraction which can lead to their detachment and death, Tetrodotoxin (1 µM Final concentration) was added to differentiation media. For MBs transduced with pLKO shRNA sequences, selection was done using Puromycin at a final concentration of 1.5 µg/mL.

RNA isolation: RNA extraction was performed using TRIzol Reagent according to manufacturer's instructions. In brief, adherent cells were lysed and scraped in 1-4 ml of TRIzol reagent, incubated for 5 minutes in RT and stored in -80°C until further processing. 200 µl chloroform was added and the mixture vigorously shaken for 20 seconds. Following a 5 minute incubation at room temperature, the mixture was then spun at 12,000 x g for 15 min at 4°C after which the aqueous phase was extracted (care must be taken to avoid contaminating interphase) and mixed with 500 µl isopropanol, mixed and incubated for 5 min at room temperature. Completely aspirate the supernatant after a 10 min spin 13,600 x g at 4°C to pellet RNA. The pellet is then washed in 70% ethanol. The pellet was then resuspended in an appropriate amount of molecular grade RNase-free water and the RNA left to solubilize at 60°C for 5 min. To eliminate trace Trizol contaminants, RNA was re-precipitated by the addition of 0.1 volumes 3M potassium acetate (pH 6.5) and 1 volume isopropanol followed by an incubation for 5 min at room temperature and pelleting by centrifugation. Following an additional wash of the pellet in 70% ethanol, the pellet was left to air dry at room

temperature and then resuspended in molecular grade RNase-free water. The quality and concentration of the RNA was then assessed using a NanoDrop 2000c to ensure 260/280 and 260/230 ratios were >2 and then processed for downstream applications.

cDNA synthesis: cDNAs were generated using Invitrogen Superscript II Reverse Transcriptase System following manufacturer's instructions. Briefly, reaction mix containing 1-2 µg of RNA , 1 µL OligoDT (500 µg/ml stock) ,1 µL dNTP Mix (10 mM stock) and NFW (upto 12 µL) was incubated in 65°C and quick chilled on ice. Further, 2µL DTT (1 mM stock), 4µL 5x First Strand Buffer and 1µL RNaseOUT were added and then incubated at 42°C for 2 minutes. Following this, 1µL of Superscript II Reverse Transcriptase Enzyme was added and the reaction mix was incubated at 42°C for 50 min before inactivating the reaction at 70°C for 15 min. The reactions are diluted in 480 µL of NFW and stored in -80°C until further processing.

qRT-PCR: 20 µl reactions containing 8.4 µl of appropriately diluted cDNA (normally serial dilutions of 5-fold), 800nM forward and reverse primers and 1x LightCycler 480 SYBR Green I Master were carried out in a 96-well LightCycler 480 Multiwell Plate. The plates were briefly vortexed and centrifuged. Polymerase chain reactions were carried out in a LightCycler 480 using the program detailed in Fig 3. Primers used are listed in Fig 3. Expression data was analyzed using LightCycler 480 Software v1.5.0.39. Primer sequences were obtained from previous publications and verified using Primer-BLAST. Primer efficiencies were then calculated using a cDNA dilution series and fit to a standard curve to ensure an efficiency range of 90%-110%

Target (°C)	Acquisition Mode	Hold (mm:ss)	Ramp Rate (°C/s)	Acquisition (per °C)
Preincubation, 1 cycle				
95		05:00	4.4	
Amplification, 45 cycles				
95		00:10	4.4	
55		00:20	2.2	
72	Single	00:05	4.4	
Melting Curve, 1 cycle				
95		00:05	4.4	
65		01:00	2.2	
97	Continuous		0.11	
Cooling, 1 cycle				
40		00:10		

Gene	Forward (5'→3')	Reverse (5'→3')
Ptn	AATGTGACCTCAATACCGCC	TCTCCTGTTTCTTGCCTTCC
Efna5	CTCCAGTATCCTTTCGCTGTG	AGCAGTAATTGTGGCCTTGG
Cxcl1	ACCCAAACCGAAGTCATAGC	GGACCCTCAAAAGAAATTGTATAGTG
Ppapdc3	CAAGCTCATTGGCATCACAG	CAGGGCTGGTCTCATATGG
Nid1	TTGGCAATCCTACTGTTCCTC	GTTAGGTGGATCTCTGGTGTT
Rps29	GAGCCGACTCGTTCCTTT	TGTTCAGCCCGTATTTGC
LMNA	CTTATGCCTCCAGTGTCACAG	GGCAGGTCCCAGATTACATG
Myog	CTGCCCTGAGTTGAGAGAGAA	GAGACCTTGGTCAGACGG
Emd	TTGTCTGCCATGGACGACTATGC	TAAGAGCTGCTCTAAAACCAATACC
Sun1	CCTAGAACTGGAACTGAACCT	TCATCCTTGCTCACGAACC
Sun2	CACTCGCTACTCTCAGGATGATAA	TAGGACTCTCGAACCACAGACTC
Syne2	GAGCTGGAAGCTCTGAAGT	ATGGAGTCTATTTTGGAGTTCTGTG
Syne3	GAGCGGCCCTGGAGGCAAGGCTTC	CAGGAGCACAGCCTGATTGTCCAC

Fig 6) Top: qPCR Program for Lightcycler 480; **Bottom:** List of qPCR primers used in this study

Chromatin Immunoprecipitation:

Cross-Linking, nuclear isolation and sonication: Sub-confluent C2C12 MBs or 6-day MTs were crosslinked using 1% Formaldehyde in growth media for 10 min at room temperature with mild shaking. The reaction was quenched using Glycine at a final concentration of 125 mM for 5 min. Cells were then washed twice on ice using ice-cold 1x PBS, scraped and pelleted down at 500xg for 5 min at 4°C. Nuclei were isolated by incubating in buffer A for 10 minutes followed by ~10 rounds of gentle shearing using a Dounce Homogenizer (Thomas USA, A53957). Efficiency of cell lysis was estimated by observing a small aliquot of the sample under the microscope for free nuclei. The nuclei were pelleted at 800xg for 5 min at 4°C and further lysed in lysis buffer B. Chromatin was fragmented by sonication using 30 cycles of 30 seconds ON/ 30 seconds OFF - High power using Diagenode BioRuptor to an average size of 150-600 bp. Samples were spun down at 16000xg for 10 min at 4°C to get rid of cell debris. To visualize fragment size, purified and de-crosslinked samples were run on 1% agarose gel.

Protein A/G Dynabeads blocking: 30 µL/ChIP reaction of beads were blocked using 1mg/ml BSA and 100 µg/ml sheared salmon sperm DNA in Buffer C for 2 hours in the cold room using the rotating mixer, washed once with Buffer C for 5 minutes and resuspended in appropriate volume of Buffer C before pulldowns.

Immunoprecipitation: Chromatin concentrations were estimated using NanoDrop 2000c using Buffer B as blank. 30-50 µg of chromatin was used per ChIP. Chromatin was diluted tenfold in Buffer C while a separate aliquot of chromatin was taken as 1% input. Chromatin was precleared using pre-blocked Dynabeads for 30 minutes in a cold room using the rotating mixer. 3-5 µg of Rabbit Anti-H3K9Me3 antibody (Millipore 07442) or Normal Rabbit IgG was added to the samples and ChIP-ed overnight in the cold room. The following day, 30 µL of preblocked beads were added to the samples for 1 hour, bound to magnetics stands and washed sequentially in low salt buffer, high salt buffer, LiCl buffer and low salt buffer for 5 minutes each. DNA was eluted from beads using 200 µL Elution Buffer for 30 minutes at 30°C 750 rpm in a thermomixer. 100 µg/ml RNase A was added to the samples and further de-crosslinked overnight in 250mM

Nacl at 65°C. The following day, samples were treated with Proteinase K with Tris-EDTA for 2 hours at 45°C. Samples were purified using QiaQuick PCR Purification Kit and eluted in 60 µL of NFW. 2 µL of eluted sample was used as template for qPCR.
Primer Design: Genomic DNA sequence for Nid1 was obtained from Ensembl and visualized on SnapGene. Primer pairs were designed and were verified for specificity using Primer-BLAST. Sonicated MB genomic DNA was used to verify primer efficiency

Region	Forward (5'→3')	Reverse (5'→3')
Nid1 Promoter	TTCTAGGGTGGGTTCTGTCC	CCAGCATTCCGGATCCAAC
Nid1 Intron	AGCTGCCTTTTACAAGCCTT	GGACAAAGAAACAGTGGAATGC
Nid1 Exon	CTCAGGTTGGGGTAGGACTT	CGAACCACTACTAGAAATGCCC
Efna5 Promoter	AGGAGGAGCGGGTCTTGCTTC	GACAAGCTAGCAGGAGAAATCC
Efna5 Intron	ACACCGCCAAGTCGGTCTAG	CTAGACGCTGTCGCAGGTAAC
Ankrd1 Enhancer	GGTAAGGTAAAGGTTGGAGATCTGAT	GGCTTGTCTGGGATTTCTTCTGT
GAPDH Promoter	CCAATGTGTCCGTCGTGGATCT	GTTGAAGTCGCAGGAGACAACC
DHFR Promoter	GCCTAAGCTGCGCAAGTGGT	GTCTCCGTTCTTGCCAATCC
Major Satellite Region	TGGAATATGGCGAGAAAACTG	AGGTCCTTCAGTGGGCATTT

Fig 7) List of primers used for ChIP-qPCR study

Buffers: Buffer A (Modified Farnham Lysis Buffer): 75mM KCl, 0.5% NP40, 0.5mM DTT, 50mM Tris pH 8, 2mM EDTA pH 8, 10% Glycerol, Protease Inhibitor Mix (1 mM PMSF, 1µM Pepstatin, 20 µM Leupeptin, 2 µg/ml Aprotinin)
Buffer B: 1% SDS, 10mM EDTA pH 8, 50mM Tris pH 8, Protease Inhibitor Mix (1 mM PMSF, 1µM Pepstatin, 20 µM Leupeptin, 2 µg/ml Aprotinin)
Buffer C: 0.5% NP40, 200mM NaCl, 50mM Tris pH 8, Protease Inhibitor Mix (1 mM PMSF, 1µM Pepstatin, 20 µM Leupeptin, 2 µg/ml Aprotinin)

Low Salt Wash Buffer: 0.1% SDS, 0.5% NP40, 2mM EDTA pH8, 150mM NaCl, 20mM Tris pH8

High Salt Wash Buffer: 0.1% SDS, 0.5% NP40, 2mM EDTA pH8, 500mM NaCl, 20mM Tris pH8,

LiCl Wash Buffer: 250mM LiCl, 0.5% NP40, 1mM EDTA pH8, 20mM Tris pH8, 0.5% Sodium-Deoxycholate

Elution Buffer: 1% SDS, 100mM $NaHCO_3$

Immunofluorescence: Adherent cells were grown on coverslips and washed in PBS to remove cellular debris and remaining serum prior to fixation with 4% paraformaldehyde (PFA), 1X PBS for 10 minutes at room temperature. Following fixation cells were washed twice in 1X PBS. Cells were then permeabilized for 10 min with 0.5% Triton-X-100 in 1X PBS and then washed 3 times in 1X PBS. Coverslips were blocked in 4% Bovine Serum Albumin (BSA), 1X PBS for 20 min at RT and subsequently incubated with the appropriate primary antibody (dilutions listed in Table). Following 3 washes in 1X PBS, coverslips were incubated with secondary antibodies conjugated with Alexa Fluor® dyes. Post washing, coverslips were incubated in 4,6-diamidino-2 phenylindole, dihydrochloride (DAPI) at a final concentration of 2 µg/ml (1:2,000). Coverslips were then extensively washed in PBS multiple times over the course of 15 min and then mounted on coverslips with Fluoromount G (EM Sciences).

Primary antibodies: Rabbit anti-H3K9Me3 (1:200) - Millipore 07442
Mouse anti-Nup153 (1:500) - Abcam 24700
Rabbit anti-H3K27Me3 (1:200) - Diagenode CS069100

BAC Isolation: Machery-Nagel NucleoBond® Xtra Midi Plus kits were used to isolate BACs from 200-300 mL dense bacterial cultures according to manufacturer's instructions.

Nick Translation: Reaction mix (Add in the same order):

10X Nick Translation Salts: 0.5 M Tris pH7.8, 0.05M MgCl2, 0.01M BME, 500ug/ml BSA

10X NTS		4ul
0.5mM dATP	Promega	5ul
0.5mM dCTP	Promega	5ul
0.5mM dGTP	Promega	5ul
Bio-16-dUTP (if using digoxigenin then dig-11-dUTP 1.5ul + 0.5mM dTTP 2ul)	Roche #14687540 (Biotin) Roche #11950520 (Dig)	5ul
Template DNA (BAC)		3-4 µg
DNase 1 (Dilute 1:25 in cold NFW - 0.33 U/reaction final conc.)	Roche #04716728001 (10U/ul)	1ul of the diluted enzyme
DNA polymerase 1 (10U/reaction final)	Invitrogen #18010-017 (10U/ul)	1ul

The reaction volume was made to 40 µL, incubated at 16°C for 90 min and heat inactivated for 75℃ for 10 minutes. A small aliquot is run on a gel to visualize a smear of 200-700 bp which confirms that nick translation has worked. Labelled fragments were then purified using radiolabeled DNA purification Sephadex G-50 Quick Spin Columns (Roche #11273973001) according to manufacturer's instructions.

3D/2D Intermediate FISH: C2C12 MBs and MTs were cultured on coverslips and fixed in 4% PFA. Immunofluorescence was first performed as described in the previous

section, using 1% BSA instead for blocking. Antibodies were fixed in 4% PFA, 1X PBS for 2 min in RT. Cells were pre-equilibrated in 2X SSC and treated with RNase A (100µg/ml) in 2X SSC at 37°C for 1 hr. Following washing in 2X SSC, cells were dehydrated with a 70%, 90% and 100% ethanol series. Coverslips were then air dried, heated to 70ºC for 10 min in an oven and then submerged into 1ml of 85°C preheated Denaturation buffer (70% formamide, 2X SSC, pH 7.0) for 20 min in a water bath. Denaturation buffer was then completely but rapidly removed and a second ethanol dehydration series was then immediately performed using -80ºC 70% EtOH for the first step followed by RT 90% and 100% EtOH. Probe solutions were prepared by resuspending 5-10 µL precipitated probe, 5 ug of sheared salmon sperm and mouse Cot-1 DNA in Hybridization buffer (2x SSC, 50% Formamide, 10% Dextran Sulphate, 1% Tween) and then denatured at 90ºC for 10 min, partially re-annealed at 42ºC for 10 min and were then deposited on slides onto which air dried coverslips were inverted. Hybridization reactions were then sealed with rubber cement and left to anneal at 37°C overnight in a humidified chamber. After incubation, rubber cement was removed and extracted coverslips were washed four times of 2 min each in 4X SSC at 45ºC followed by four times of 2 min each in 0.1X SSC at 60ºC. Coverslips were then pre-equilibrated in 2X SSC, 0.1% Tween-20 and blocked with 4% BSA, 2X SSC for 20 min. Following blocking, biotin-labelled probes were detected by incubating coverslips for 1 hour at room temperature with 1:500 Alexa Fluor 488/568-conjugated Avidin/Streptavidin (Invitrogen). Digoxigenin-labelled probes were similarly detected by an Alexa Fluor 488/647 conjugated mouse anti-digoxigenin antibody. Coverslips were subsequently washed 3 times in 4X SSC, 0.1% Tween-20 at 37ºC and mounted on slides in Vectashield (Vector Labs). For biotin and digoxigenin-labelled probes, DNA was then directly stained with DAPI (1:20000) for 7 min and then washed with 1X PBS for an additional 10 min. Coverslips were then mounted on slides with Vectashield.

2D FISH: C2C12 MBs and MTs were trypsinized and spun down. The nuclei were then isolated using Modified Farnham Lysis buffer and a Dounce homogenizer. 3:1 Methanol:Acetic Acid was then added dropwise to the nuclei pellet while vortexing gently. Fixed nuclei were then dropped onto wet slides from a height of at least 1.5 feet,

dried and processed for FISH like previous protocol, albeit using coplin jars compatible with slides.

Dataset processing:

Microarray analysis: Microarray experiments to analyze global gene expression patterns were performed as described by Robson et al., 2016 and analysis was done with the help of Dr. Jose I. De Las Heras. Briefly, data was quantile normalized, stored as SEG files and visualized on Integrative Genomics Viewer (IGV) by Broad Institute.

DamID analysis: $\log_2$(Lamin B1/soluble Dam) values were obtained from sequencing reads, quantile normalized and represented as DamID scores by Dr. Jose De Las Heras (as described by (Robson et al., 2016)). LADs were identified using circular binary segmentation algorithm DNACopy (Seshan VE and Olshen A (2016); R-package version 1.46.0) using default parameters. To identify LADs unique to MBs and MTs, bedToolsIntersect was used to identify unchanging LADs which were then subtracted using bedToolsSubtract to obtain unique MB and MT LADs.

ChIP Seq Analysis: HOMER v4.11 ChIP Peak calling algorithm (peak length parameter was set as variable) was used on publicly available BigWig datasets on GEO Accession if BED files representing peaks were not available.

Hi-C Analysis: - Hi-C experiment was performed by Dr. Michael Robson and I processed and analyzed aspects of it with the guidance and assistance of Dan Robertson. In brief, HiCPro packages were used to filter invalid reads, assigned to restriction fragment (which was performed by Dan Robertson) and aligned to mouse mm9 genome. Valid interaction pairs were used to construct .cool contact matrix, normalized using Iterative correction (ICE) at suitable resolution and visualized on HiGlass. Around 250,000,000 valid read pairs were obtained per replicate. To identify A/B compartments, findHiCInteractionsByChr.pl package in HOMER v4.11 was used and the first eigenvector (PC1) was visualized on IGV.

Results:

1) Characterization of genome organization changes during myogenesis

1.a) Analysis of global LAD rearrangement and its relation to gene expression during myogenic differentiation

In order to obtain a comprehensive LAD map of the myogenesis system, LADs were extracted from previously generated DamID scores. Previous analysis conducted by the lab used larger genomic windows (with an average size of ~450 Kbp) to identify regions which reposition differentially with respect to the NE during myogenesis, termed as 'Interior to Peripheral Regions' for regions moving towards nuclear periphery in MT and 'Periphery to Interior Regions' for regions moving away from nuclear periphery in MT (Robson et al., 2016). This method allowed identification of statistically confident repositioning regions in the absence of biological replicates and/or poorer sequencing depth. However, more recent studies have shown that such an approach fails to identify a significant fraction of smaller repositioning regions. Thus, to obtain a finer map of the genes under NE regulation, we identified LADs (of average size ~30 Kbp) which are unique to MB or MT and mapped the genes under their regulation. Figure 8a shows the representative IGV tracks for 3 classes of regions, non-unique LADs (*Zfp80fb* gene), MB unique LADs (*Titin* gene) and MT unique LADs (*Cdk14* gene). To verify if DamID defined LADs accurately reflected the radial positioning of the region, 2D FISH was performed for a MT unique LAD region (*Nid1* gene) which showed significantly increased proximity to nuclear periphery (Fig 8b), showing that 2D FISH can be used to study changes shown by DamID in line with several published studies. The observed change in spatial distribution profile for *Nid1* loci by 2D FISH matches with previous observation using 2D-3D intermediate FISH by Robson et al, with ~40% increase in number of loci less than 2 microns from the nuclear periphery during myogenesis.

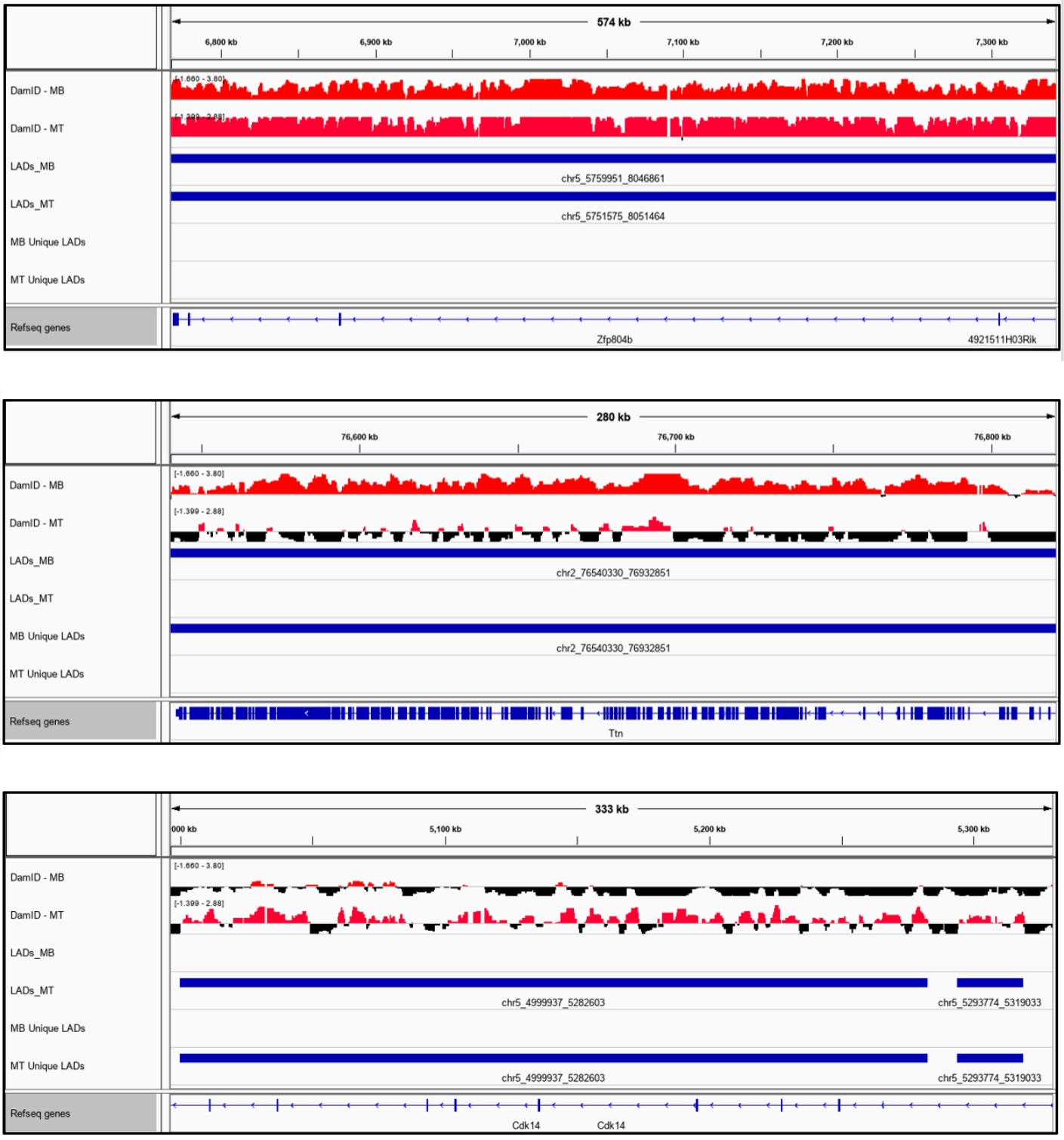

Fig 8a) IGV tracks for 3 classes of LADs (top: Unchanging, middle: MB unique, bottom: MT unique) along with DamID scores. Positive DamID scores (increased Lamin B1 association) in red, negative scores (decreased Lamin B1 association) in black. Normalized to soluble Dam.

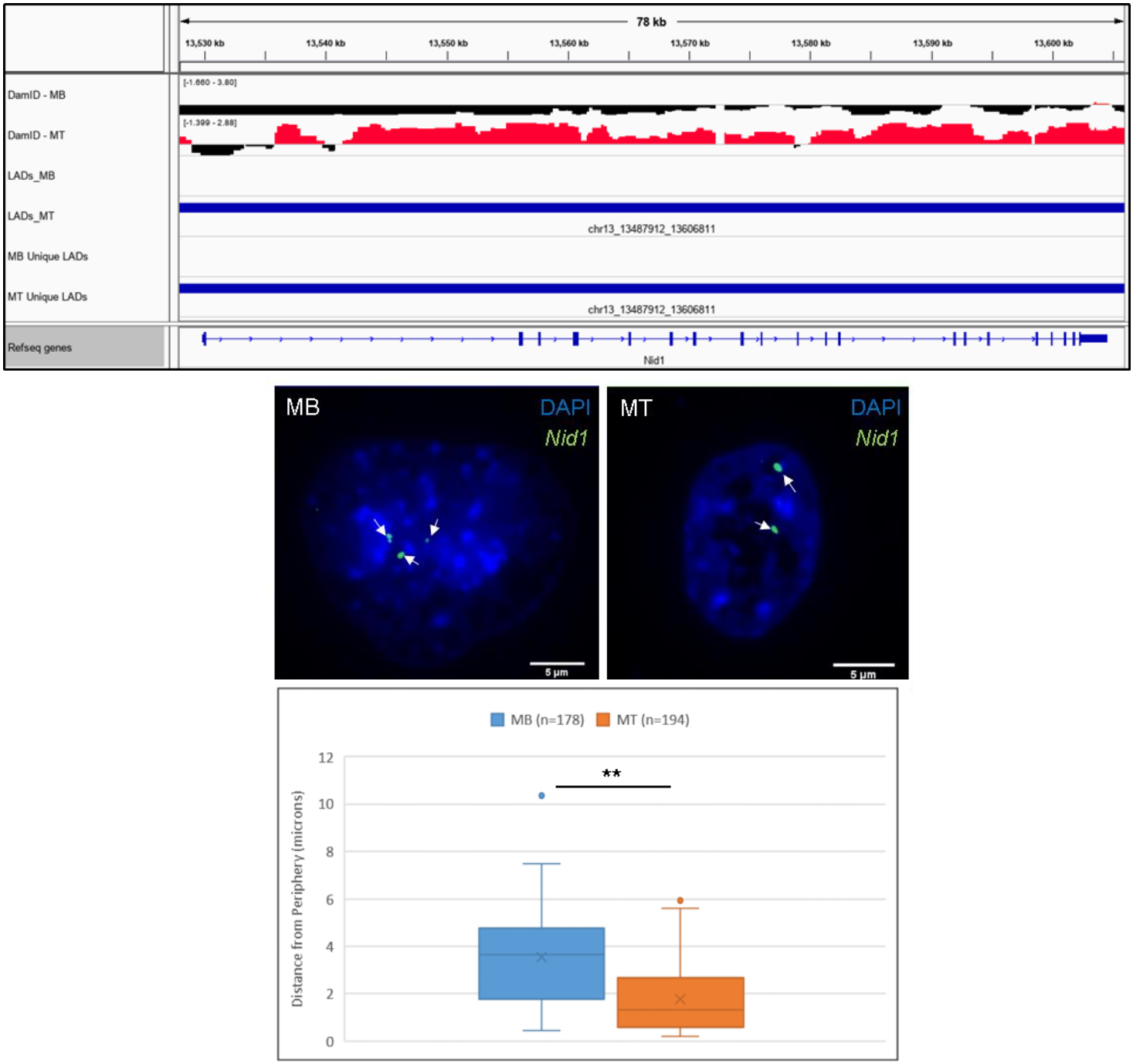

Fig8 b) Verification of LAD status of *Nid1* by 2D FISH. Top: IGV track for *Nid1* region Bottom: 2D FISH representative images with quantification of nearest distance from DAPI edge for MB and MT, significance test using Mann-Whitney (pooled data from N=2, ** = p<0.05)

By comparing genome regions encompassed by LADs to gene positions, a list of genes overlapping with LAD regions unique to MB or MT was generated. Analysis revealed that 3219 genes were in LADs unique to MB (i.e. genes that lose LADs during differentiation) while 3441 genes were in LADs unique to MT (i.e. gain LADs during differentiation). Around 38% of the genes which gain LAD status upon myogenic differentiation get repressed while ~13% of the genes get activated (Fig 9a). Similarly, around 35% of genes that lose LADs during myogenesis tend to get upregulated while ~12% get repressed (Fig 9b). Interestingly, a large fraction (~50%) of genes do not show any change in expression in both classes, suggesting that transcriptional repression was not a feature shared by all LADs. It is possible that LADs with repressive functions have special characteristics like association with a transcriptional repressor.

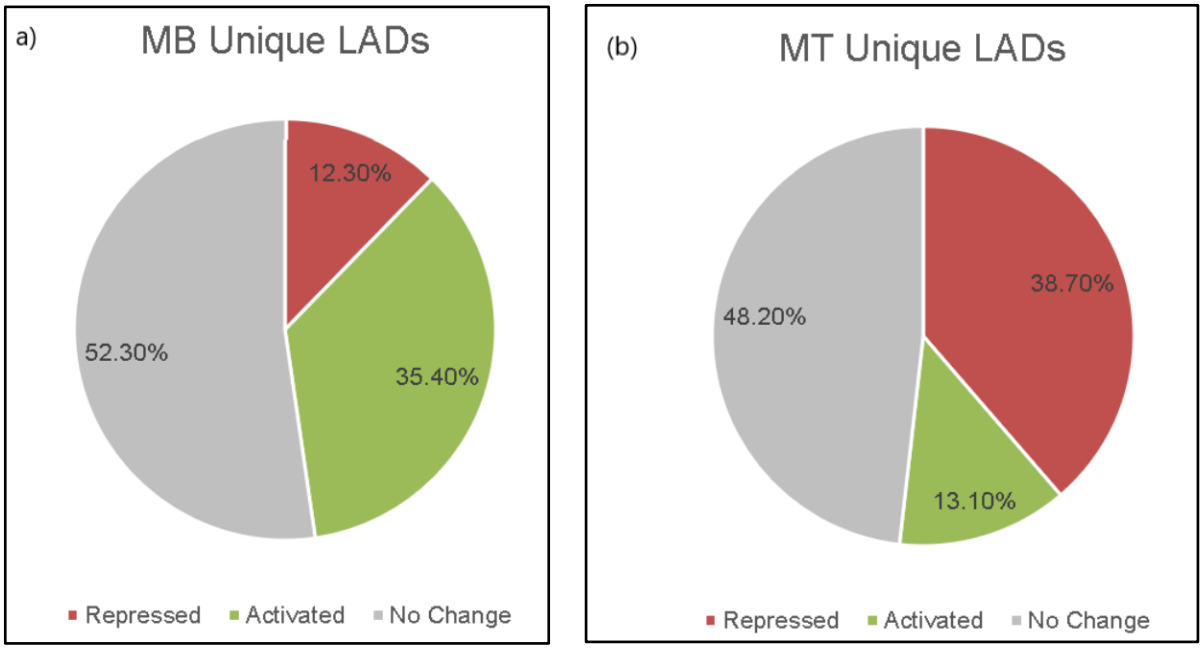

Fig 9) Pie chart depicting distribution of microarray expression profiles of genes during myogenesis under regulation of **a)** MB Unique LADs and **b)** MT unique LADs

To understand the importance of genes which show LAD rearrangement during myogenesis, Gene Ontology (GO) Analysis was performed on extracted genes having unique MB or MT LADs. Results show that genes important for muscle development and morphogenesis (‘pro-myogenic genes’) tend to move out of LADs (Fig 10a) while genes important for repression of cell cycle and metabolism (‘anti-myogenic genes’) tend to move into LADs upon differentiation (Fig 10b). This result suggests that LADs play a critical role in regulating myogenesis.

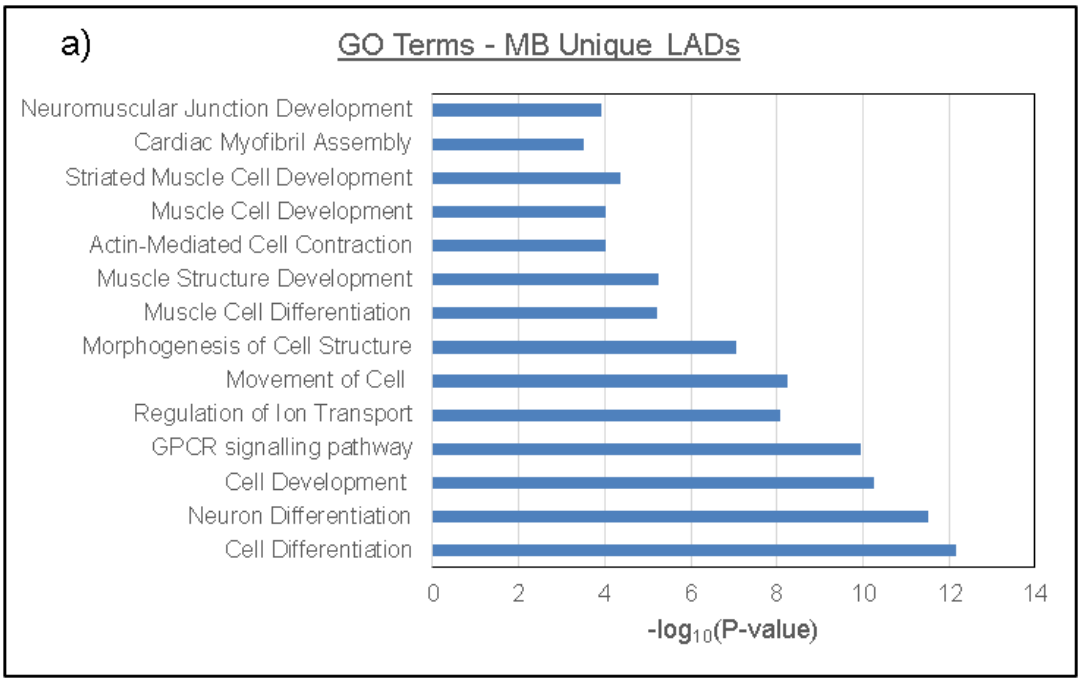

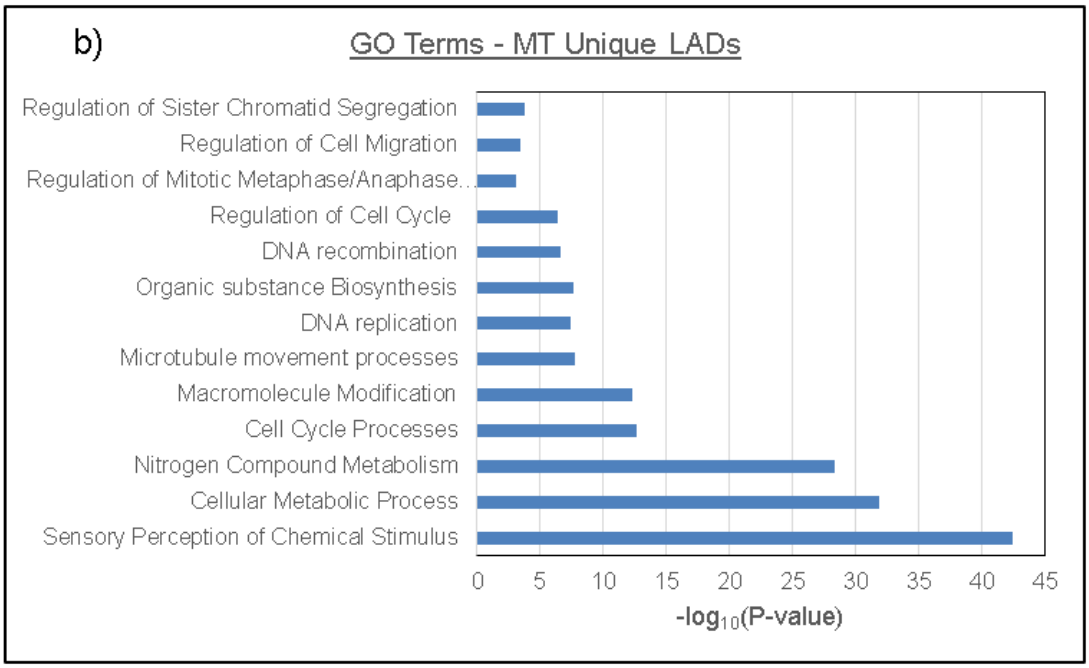

Fig10) GO Term Enrichment Analysis for genes under regulation of **a)** MB Unique LADs **b)** MT Unique LADs- Selected Top Categories ($p<0.001$ and FDR<0.05 was considered as significant)

The total genomic region under regulation of either MB unique or MT unique LADs (~245 Mbp) identified by my analysis was significantly lower than the total genomic region which reposition during myogenesis as identified by Differential Region Analysis (~800 Mbp) by Robson et al., which was expected as the latter identified large chunks of genomic regions that move in a coordinated fashion. Counterintuitively, the number of genes identified by my analysis were significantly higher than those found by Robson et al. We verified that this was due to identification of several smaller novel regions under LAD regulation which were previously missed by Robson et al., 2016 (summarized in Fig 11)

	Average Size (Kbp)	Number* (#)	Total Size (Mbp)	% of Mouse Genome	Genes (#)
MB Unique LADs	32.1	4842	99.5	3.98	3219
MT Unique LADs	30.9	6028	145.3	5.8	3441
Interior to Periphery Differential Region	416	713	280	11.2	2197
Periphery to Interior Differential Region	539	1034	525	21.0	2939

Fig 11) Summary table detailing comparisons between LAD features identified by my analysis and Differential Region Analysis by Robson et al.

To understand the importance of the additional genes found in my analysis .i.e., which change LAD status but were not identified as a part of differentially repositioning region in Robson et al., 2016 study; expression data was extracted and GO Analysis was performed. Interestingly, 73% of the additional genes found in my analysis did not show any change in transcriptional profile. Further, GO Analysis of these genes did not show an enrichment for a specific biological process. This result seemed to suggest that genes important for myogenesis tend to reposition as larger units (which are identified reliably by Differential Region Analysis) concomitant with change in transcription. Upon further inspection, we found that a significant fraction of these additional genes identified in my analysis lacked any Functional GO Term Association and had poorly characterized biological functions. Further, several of these were not even annotated in the mm9 mouse genome/Refseq gene database and lacked gene expression data in our microarray. Interestingly, several miRNAs and lncRNAs were identified to be underlying in the additionally mapped LAD regions, suggesting that regulatory elements are likely to be under positional control of LADs. Several previously characterized pro-myogenic miRNAs miR-133, miR-125b, miR1a-1, miR1a-1hg and miR1a-2, which

negatively regulate proliferation (reviewed in Yeijing Ge et al., 2011), move out of LADs in MT. For example, Sox2ot (long non-coding RNA) and Mir1897 (microRNA) were identified as novel genes in my list. These genes lie within a 4 Kbp region and were thus missed by Differential Region Analysis although this gene moved into a LAD in MT (Fig 12a). Interestingly, Mir1897 is not annotated in the mm9 genome but was identified as lying in the same genomic locus as Sox2ot indirectly by liftover from the mm10 mouse genome (Fig 12b).

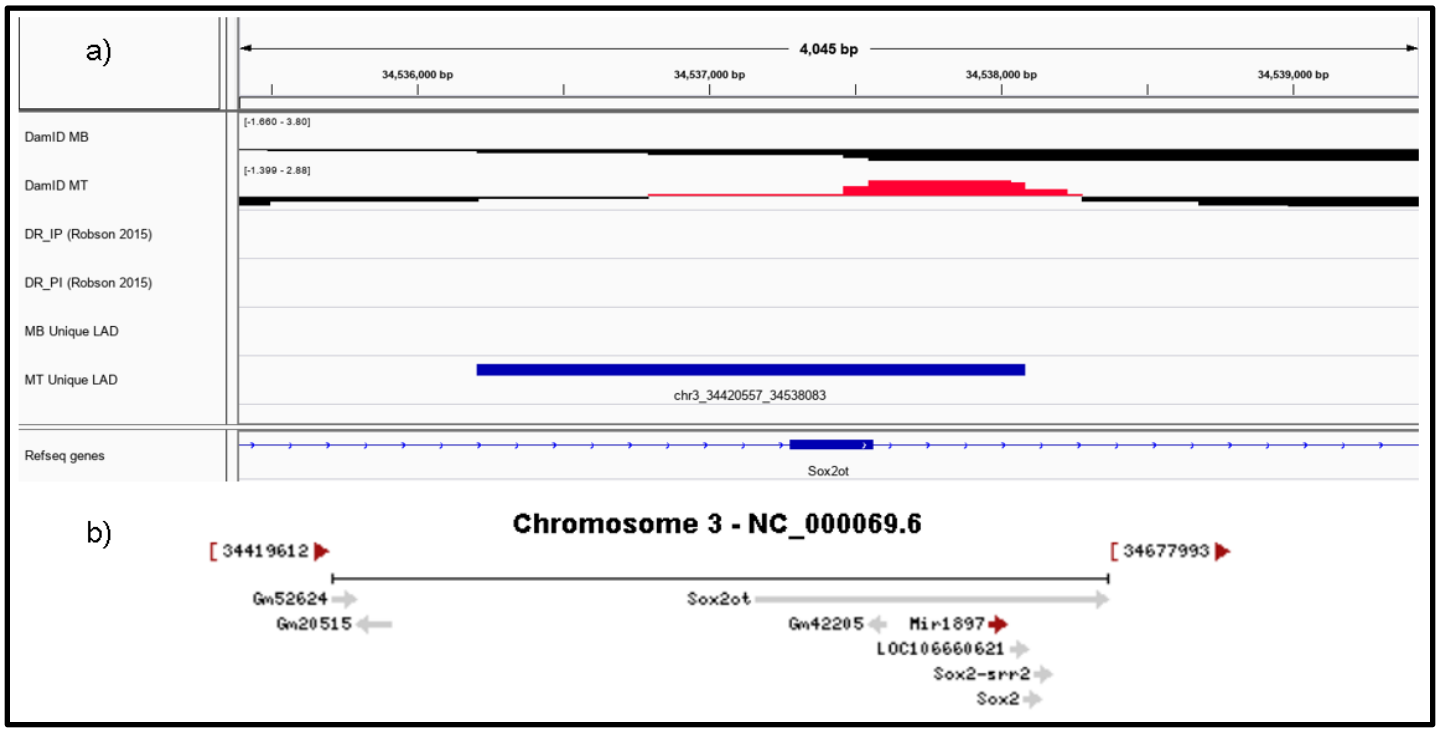

Fig 12) Regulatory RNAs under LAD regulation **a)** Representative IGV Track of Sox2ot and Mir1897 regulatory RNA encoding 4 Kbp region identified uniquely in my analysis. Positive DamID scores (increased Lamin B1 association) in red, negative scores (decreased Lamin B1 association) in black. Normalized to soluble Dam. **b)** NCBI mm10 representation of Sox2ot genomic locus. Note that Mir1897 is not annotated under Refseq genes

Further, to understand if enhancers are under the regulation of LADs, we extracted MB and MT specific enhancer coordinates (of average size ~5 kbp) from Blum et al. 2012 using enhancer specific histone modifications and contrasted them with MB and MT Unique LADs. Analysis revealed that 252 MB specific enhancers moved into LADs while

283 MT specific enhancers moved out of LADs during myogenesis, further indicating that regulatory elements are LAD control.

1.b) Analysis of global chromatin compartments during myogenic differentiation

To understand how spatial repositioning of genes affect their higher order genome organization, we studied correlations between DamID and Hi-C datasets. Genome-wide contact matrices were generated for MB and MT and represented as a heat-map of contact frequencies. The Hi-C contact matrices were then processed using Principal Component Analysis (PCA) to partition the genomic regions into 2 arbitrary compartments depending on their self-interaction contact frequencies and referred to as A and B compartments (Lieberman-Aiden et al., 2009). In general, the A compartment is euchromatic and is transcriptionally active while B compartment is heterochromatic and transcriptionally inactive. These compartments were then functionally annotated by comparing with publicly available ChIP-seq datasets for active and inactive histone marks. These A and B compartments represent an averaged view of large-scale chromatin loops within which genomic interactions are favoured. Whole genome view of the normalized contact matrices showed that there are no apparent large-scale genome organizational changes, suggesting that overall chromosome territoriality is conserved during myogenesis (Fig 13 a,b). Interestingly, overall interaction frequencies appeared to be higher in MTs. Further, certain chromatin compartments appeared to be sharper or more insulated in MT (Fig 10 c,d; regions marked by arrows, compared to unchanging contact frequencies in regions not marked by arrows), suggesting a reduction in contact frequencies with regions outside a given compartment (.ie. reduced trans interactions). This could be partly explained if one of the two interacting regions within the same compartment undergoes a chromatin compartment switch, therefore leading to reduced interactions between them.

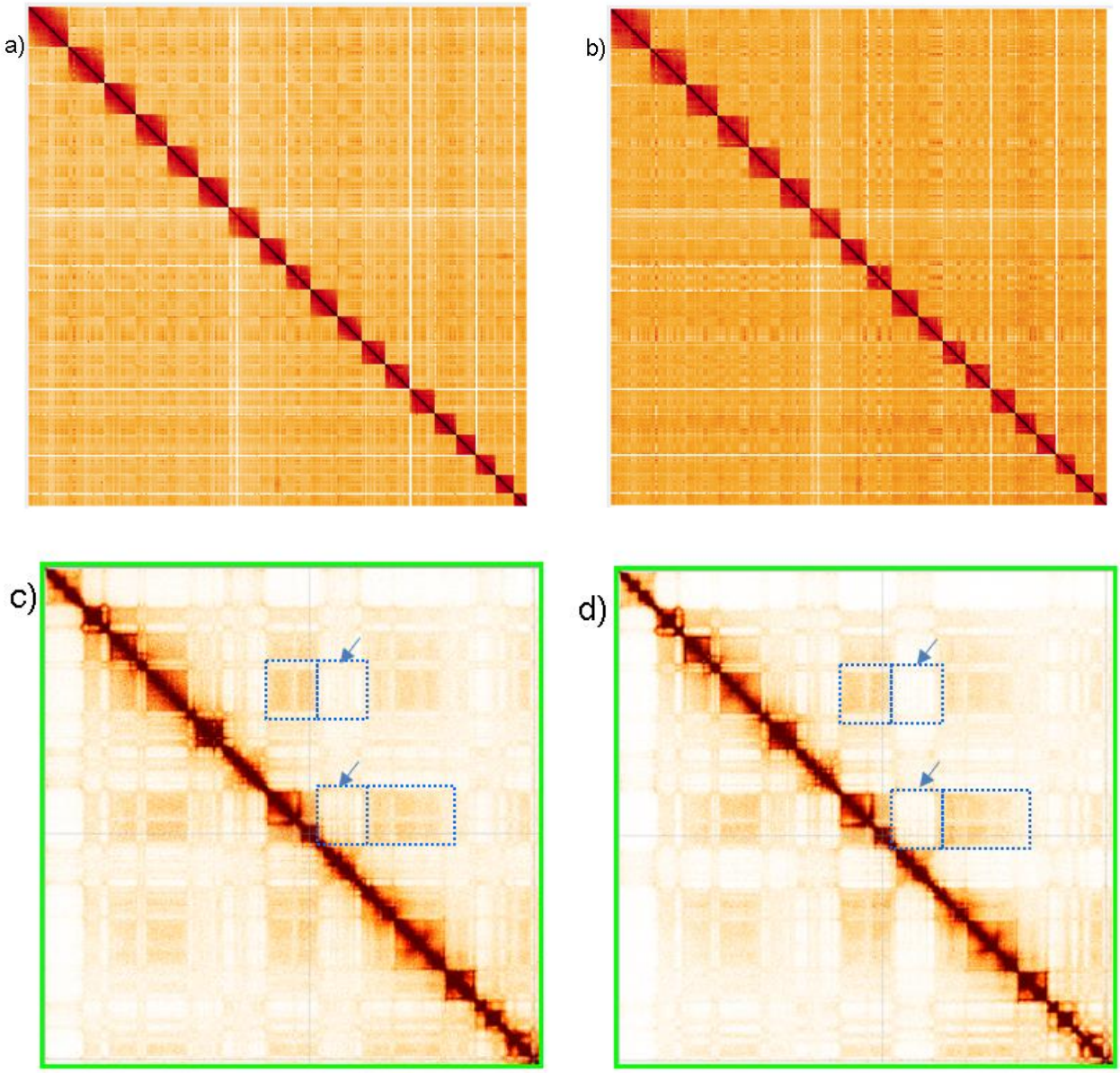

Fig 13) Hi-C Contact Maps viewed on HiGlass. Whole genome view of Hi-C contact frequencies for **a)** MB and **b)** MT. Chr 11 region showing plaid pattern of interactions representing chromatin compartments for **c)** MB and **d)** MT. Reduced contact frequencies are observed in compartments marked by arrows in MT compared to MB.

Further, we identified genomic regions which transition compartments during myogenesis by analyzing the sign of the Principal Component 1 (PC1) Eigenvector which defines the compartments (Fig 14c).

Interestingly, Nidogen 1 (*Nid1*) and Ephrin A5 (*Efna5*), two of the several previously characterized genes whose transcriptional repression was shown to be crucial for myogenesis show an A to B compartment shift while moving into a LAD upon differentiation (Fig 14b). These genes were confirmed to reposition to the nuclear periphery in MTs by 2D FISH at different stages of the project (Fig 8b and 24b). On the other hand, Titin (*Ttn*), which is known to be important for myogenesis, shows the opposite behaviour of strongly switching from B to A compartments concomitant with its transcriptional upregulation and moving out of a LAD (Fig 14a)

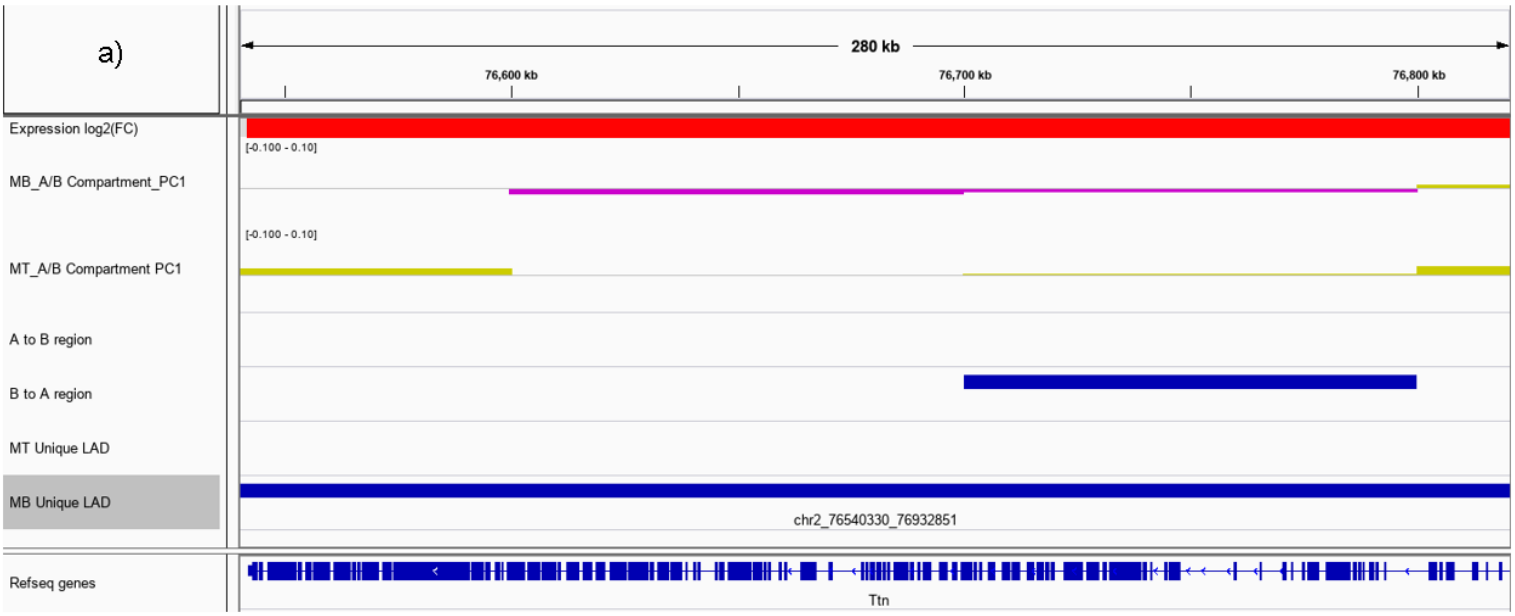

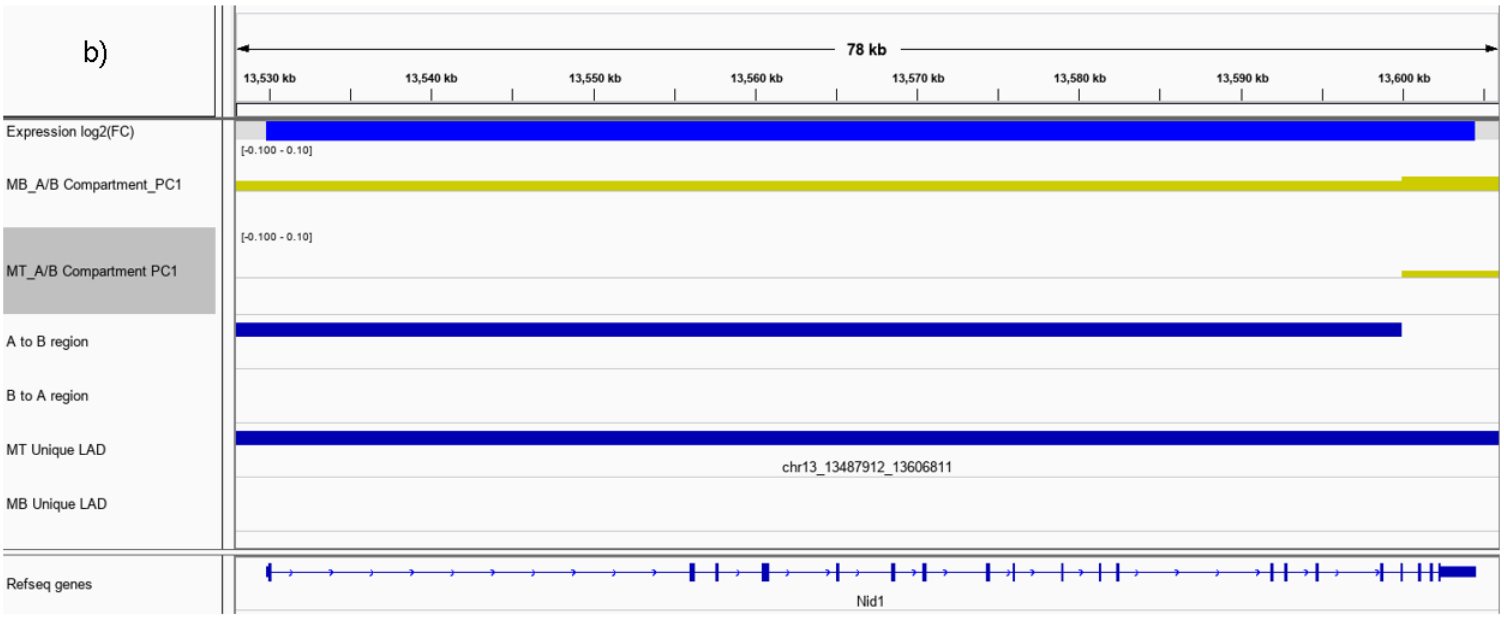

c)

	Number* (#)	Total Size (Mbp)	% of Mouse Genome
A to B regions	570	57	2.3
B to A regions	1173	117.3	4.7

Fig 14) IGV tracks representing Microarray Expression data (log_2(MT/MB)), MB and MT PC1 values, A-B and B-A compartment switching regions, MB and MT unique LADs for **a)** Titin and **b)** Nid1 genes. **Key**-- Microarray: Blue- Downregulated, Red-Upregulated; PC1 values: Yellow-Positive/A compartment, Pink- Negative/B compartment **c)** Summary of regions identified as undergoing an A-B and B-A compartment switch.

Visualizing a larger 5 Mbp region, several interesting observations can be made regarding correlation between LADs and A/B Compartments that reorganize during myogenesis (Fig 15). For instance, in region 1, we can observe a strong B to A compartment transition during myogenesis which correlates with the loss of LAD. In region 2, the opposite behaviour is observed where the genomic region transits to the B compartment from A which also correlates with formation of several new LADs in MTs. This region also includes the previously characterized Nid1 gene, whose transcriptional shutdown and peripheral tethering is known to be NET39 dependent (Robson 2015). Region 3 also mirrors the compartment transition and LAD restructuring behaviour of Region 1, suggesting a large-scale rewiring of genomic contacts during relocalization to nuclear periphery.

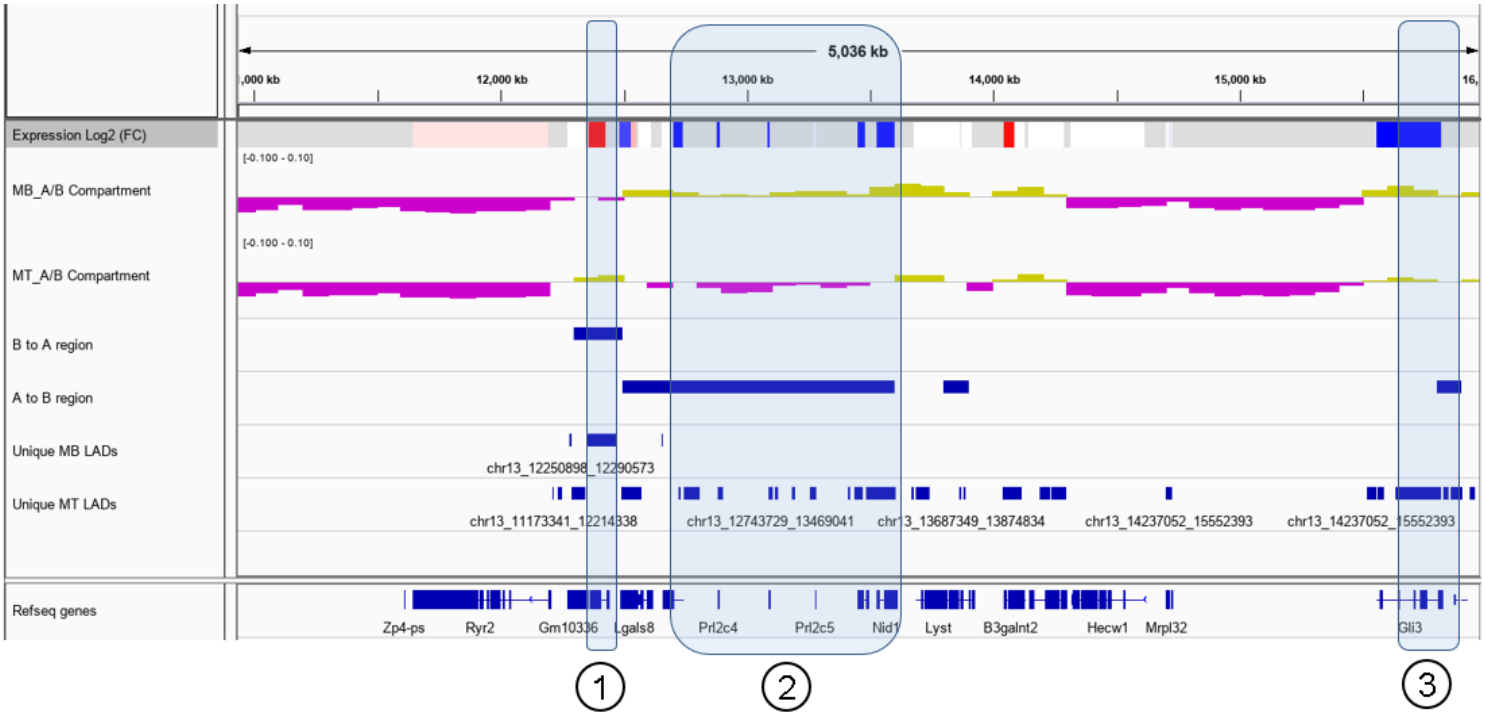

Fig 15) IGV visualization of 5 Mbp region on Chr 13 representing Microarray Expression data (log_2(MT/MB)), MB and MT Compartment PC1 values, A-B and B-A compartment switching regions, MB and MT unique LADs. **Key**-- Microarray Expression: Blue- Downregulated, Red- Upregulated; PC1 Compartment values: Yellow- Positive/A compartment, Pink- Negative/B compartment

Following our observations of the 5 Mbp region, we sought to understand the global implications of compartment switching. Genes associated with genomic regions undergoing a A to B compartment switch (or vice versa) were identified. Interestingly, the number of genes switching compartments (2224) were ~3-fold lesser than the number of genes switching LAD status (6660), although the total size of genomic regions undergoing compartment switching (175 Mbp) was comparable to the total size of genomic regions undergoing LAD restructuring (245 Mbp) (summarized in Fig 16a) Since some of the previously characterized pro-myogenic genes (*Ttn*) and anti-myogenic genes (*Nid1, Efna5*) switched compartments, we asked if compartment switching was globally associated with pro- and anti-myogenic genes. GO Enrichment Analysis was performed on genes which switch compartments to see if they enrich for a particular biological process. GO analysis revealed that genes that undergo a B to A compartment switch do not significantly enrich for pro-myogenic pathways while genes undergoing an A to B compartment switch do not enrich for anti-myogenic pathways, suggesting that most myogenesis responsive genes were already in their respective A or B compartments.

To understand if loss or gain of LADs correlated with compartment switching, we correlated the compartment status of a gene with its LAD status and transcriptional profile (summarized in Fig 16a). We observe that genes that switch into the B compartment are predominantly repressed while genes that switch into the A compartment get transcriptionally upregulated, although genes which do not get transcriptionally altered form the majority in both classes (Fig 16b). Further, our results show that a significant fraction of genes that switch compartments (~30% for both A-B and B-A switching regions) also show a corresponding LAD switch, potentially suggesting that LADs help in maintenance of B compartments and regulate compartment switching (Fig 16c).

a)

	Total	Upregulated (#)	Upregulated (%)	Downregulated (#)	Downregulated (%)	MT unique LAD (#)	MT unique LAD (%)	MB unique LAD (#)	MB unique LAD (%)
A to B genes	894	133	14.8	270	30.4	228	25.5	55	6.1
B to A genes	1330	238	17.9	121	9.1	243	18.2	418	31.4

b)

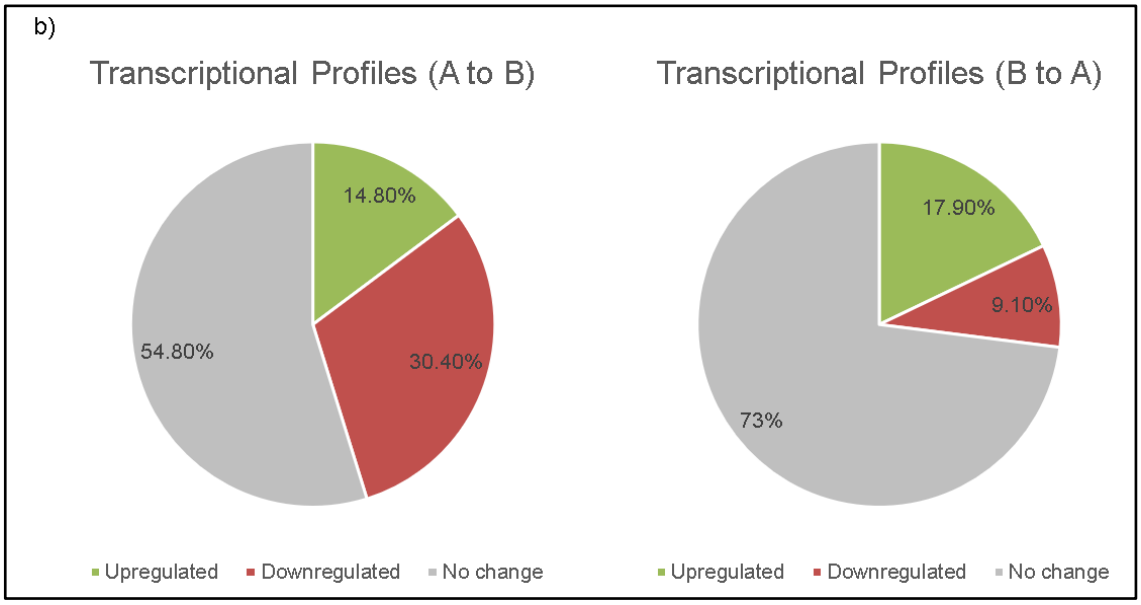

c)

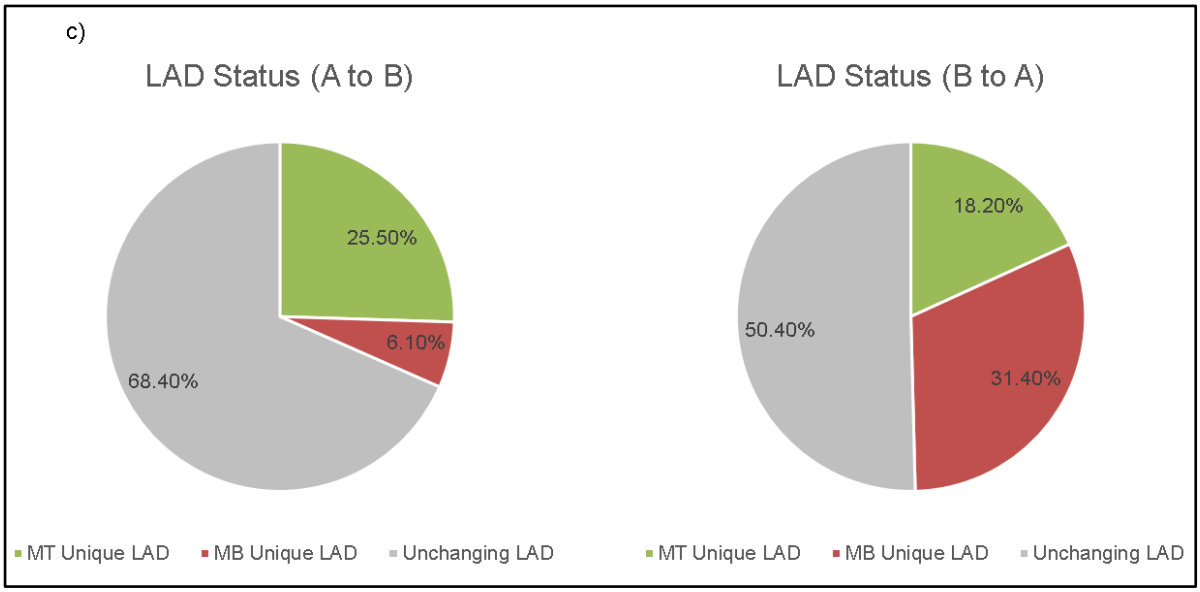

Fig 16) a) Summary table detailing LAD characteristics and transcriptional status of genes undergoing compartment switching **b)** Pie chart depicting expression trends during myogenesis for genes undergoing A-B and B-A compartment switch **c)** Pie chart depicting LAD reorganization during myogenesis for genes undergoing A-B and B-A compartment switch

2) How do NET interactions drive its functions?

Having mapped the global genome reorganization events that happen during myogenic differentiation in the first section, we wanted to study mechanisms by which these changes are exerted by the NE. We focused on the muscle specific NET39 which shows massive transcriptional upregulation during myogenesis, while other ubiquitous NE associated proteins like Lamin A/C do not change in transcription (Fig 17).

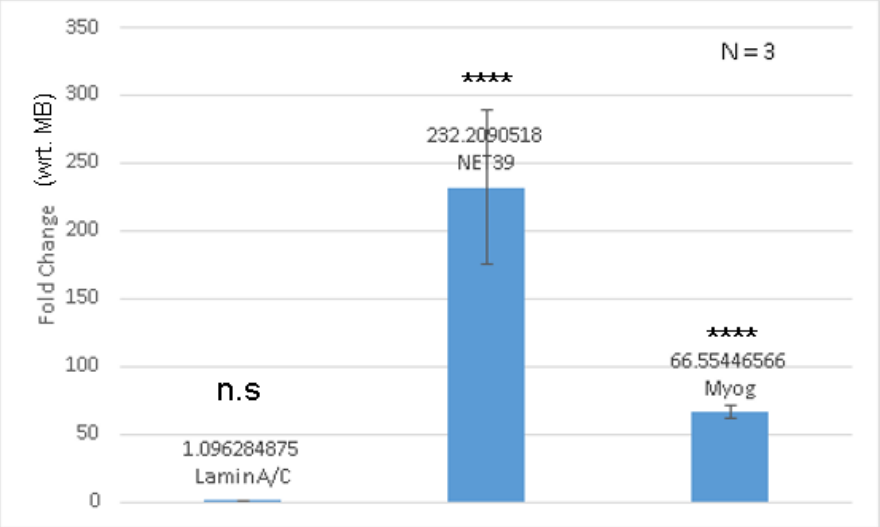

Fig 17) qPCR expression profiles of *Lmna* (Lamin A/C), *Ppapdc3* (NET39) and myogenic marker *Myog* in MT. Data normalized to MB. Students' t-test was used to test for significance (n.s = Not significant, ****=p<0.001). Error bars represent SDM.

Studies have proposed conflicting roles regarding how NET39 affects myogenesis, but more recent studies have shown that NET39 enhances repression of critical development genes by modulating their spatial organization (Liu et al., 2009; Robson et al., 2016). Several of the previously characterized genes like *Nid1* are under the spatial and transcriptional control of NET39. Further, NET39 also affects the radial positioning of whole chromosomes both in heterologous systems (Chr 5 and 13 in HT1080) and

C2C12 myogenesis system (Chr 8), suggesting that NET39 can mediate large-scale genome organization (Robson et al., 2016; Zuleger et al., 2013). However, the mechanisms by which NET39 mediates these changes are poorly understood. Further, NET39 lacks any predicted DNA or histone binding domains, hinting that its genome organization functions are likely to be indirect.

2.a) Analysis of NET39 and NET29 'Interactome' Proteomics datasets

We hypothesized that several genome organizing principles must be conserved among similar NETs and hence analyzed both NET39 and fat specific NET29 'interactome' datasets to find interesting partner proteins which could help explain NET function. The NET39 'interactome' dataset was generated by Dr. Michael Robson and was obtained by overexpressing a NET39 version fused to mutant BirA enzyme module in MBs and MTs (which promiscuously adds Biotin to proteins in the vicinity of ~10 nm) followed by mass spectrometry. On the other hand, NET29 'interactome' dataset was generated by Dr. Dzimtry Batrakou by a crosslinking-mass spectrometry approach by overexpressing wild type NET29 and a phospho-deficient version of NET29 (which lacks NET29's genome organizing functions) in preadipocytes.

The interactome datasets initially identified that NET39 interacts with ~500 proteins while NET29 is predicted to interact with over 1500 candidates. Potential interaction partners from these lists were curated according to several parameters listed below.

- GO Term Association: To identify clusters of proteins with similar GO terms, GO Enrichment Analysis was performed to identify proteins significantly overrepresented in the interaction dataset. Further, to search for specific classes of proteins (which may not form a large class), a list of proteins associated significantly with specific GO Terms were extracted using QuickGO and intersected with our dataset. For instance, top 500 proteins associated with 'Transcriptional Repression' were extracted from QuickGO and compared with NET29 interaction dataset to identify specific transcriptional repressors and epigenetic enzymes interacting with NET29 (Fig 18a).

- Absolute spectral values: Proteins which were detected with very low spectral values in all conditions were discarded. Proteins which showed zero spectral values for only one condition were given a pseudo count spectral value of ‘1’.
- Fold-enrichment over internal controls: For NET39, proteins that showed at least a 2 to 5-fold difference in interaction profiles between MB and MT overexpressed conditions were selected. For NET29, proteins that showed at least a 2 to 5-fold difference in interaction profiles between the wild type and phospho-null versions of NET29 were selected.
- Manual selection: Contaminating proteins known from literature (Keratin, for example) were manually removed. Further, since the mass-spec isn’t normalized to the abundance of the protein itself, case-by-case basis curation was done for certain proteins. For example, Lamin A is highly abundant and therefore needs an arbitrarily higher threshold to be considered as a real interaction partner while Epigenetic Enzymes like Chd1 are inherently expressed lower but are known for their high processivity and were therefore given a lower cutoff value to qualify as a significant interactor.

The curated datasets reveal that these potential partner proteins are very diverse in terms of functions and spatial localization as indicated by examples listed in Fig 18 b,c. This analysis suggested a multifaceted role for NET39 in regulating aspects of myogenesis and genome organization. We focused on a subset of these proteins as several were already linked to genome organization while others posed as novel candidates to study genome organization.

a)

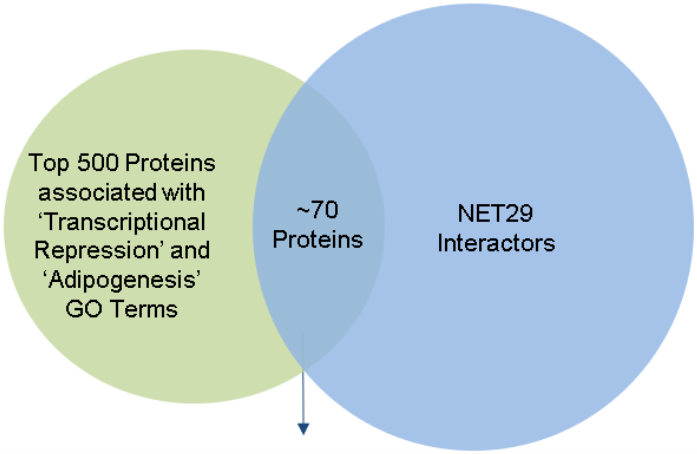

b)

NET39 Interaction Partner	Dominant Function	Spectral counts(MB)	Spectral counts(MT)
Lap2Δ	Nuclear Envelope/Chromatin Binding	206	68
HNRNPU	Chromatin Organization	52	9
Rtn4	Membrane Curvature	63	1154

c)

NET29 Interaction Partner	Dominant Function	Spectral counts (WT-NET29)	Spectral counts (Ph0-NET29)
NONO	Transcriptional Repressor	82	18
Sqstm1	Autophagy	109	10
Lamin A/C	Nuclear Envelope/Chromatin Organization	353	132

Fig 18) a) Schematic representing approach for extraction of an example partner protein class (Adipogenic Transcriptional Repressors) using associated GO terms. **b)** Representative examples of curated NET39 interaction partners with spectral counts and associated functions **c)** Representative examples of curated NET29 interaction partners with spectral counts and associated functions.

2.b) Does NET39 regulate chromocenter organization and nuclear shape characteristics?

The nucleus and chromatin packaging appear to undergo striking changes during myogenesis. Several previous studies have suggested that 'mesoscale' features of the nucleus can regulate genome organization directly or indirectly. For instance, recent studies have suggested that chromocenters, which are repeat-rich and consist of genomic 'dark matter', can help in B compartment assembly and act as an anchor to facilitate long range interactions between coding regions of the genome (Wijchers et al., 2015). Another study in rod nuclei used polymer simulations to show that strong intra-chromocenter attractive forces can drive chromocenter coalescence which can promote self-assembly of eu- and heterochromatic regions of the genome (Falk et al., 2019). One of the proteins that strongly interacts with NET39 is the HNRNPU (~5 fold decreased association with NET39 in MT) which has been shown to regulate chromocenters and chromatin condensation (Fan et al., 2018) (Kukalev et al., 2009) (Wang et al., 2016a). Further, NET39 also shows strong associations with Reticulon 4, BAR domain proteins, Fam134b, Lunapark etc., (2-18 fold increased association in MTs) which have been shown to regulate membrane organization and shape features at the NE and the Endoplasmic Reticulum across different model systems (Wang et al., 2016b), (Bhaskara et al., 2019) . Several studies have suggested interplay between nuclear topology, shape and chromatin organization in disease and development. (Anderson and Hetzer, 2007). For instance, in neurodegenerative tauopathies, alterations in shape features of NE precede heterochromatin relaxation and genome organization alterations (Frost et al., 2016). Thus, we sought to address if NET39 exploits partner protein interactions to modulate nuclear topology and chromocenter organization to drive genome organization in myogenesis. Using imaging tools, we quantified attributes like chromocenter parameters, nuclear volume, sphericity and surface area in **MB**, **shNT** (control) **MT** and **shNET39** (NET39 deficient) **MT**. NET39 expression levels in shNET39 MT are only 25% of control MT levels, as verified by qPCR (Fig 19h). DAPI signal was used to estimate the parameters. Analysis revealed that the average number of chromocenters per nuclei decreased ~2 fold (Fig 19c) while average chromocenter volume increased by ~2 fold from MB to shNT MT (Fig 19b),

hinting at a potential chromocenter coalescence. Total chromocenter volume per nuclei appeared to decrease from ~30 μm^3 in MB to ~23 μm^3 in shNT MT (Fig 19d). However, this estimate might not be reliable due to the possibility that the coalescence can result in chromocenters of higher densities but same volume. Further, no statistical difference was observed between the distributions of shNT MT and shNET39 MT for all chromocenter features (Fig 19b-d), suggesting that NET39 does not regulate features of chromocenter reorganization that occur during myogenesis.

Further analysis of nuclear shape and topology attributes revealed interesting changes that occur during myogenesis. 3D reconstruction of MB and MT nuclei showed that MB nuclei adopt a flatter, 'pancake' like shape while MT nuclei are more ellipsoidal. Quantification revealed that compared to MB nuclei, shNT MT nuclei showed increased sphericity (from ~0.7 to ~0.79, Fig 19g), decreased surface area (from ~850 μm^2 to ~735 μm^2, Fig 19e) while nuclear volume remained unchanged (~550 μm^3, Fig 19f) . Further, comparison of shNT MT with shNET39 MT showed that most topological parameters remain unchanged while nuclear volume showed a slight increase (from ~550 μm^3 to ~580 μm^3) (identified as significant by pairwise Students' t-test but insignificant by 1-way Anova and Tukey's HSD) , suggesting that NET39 does not regulate topological features of the nucleus in myogenic differentiation (Fig 19e-g).

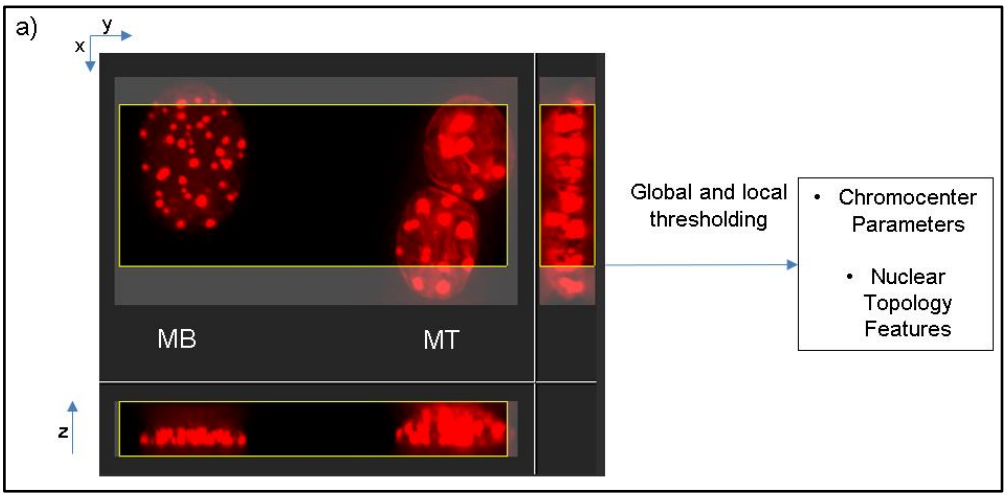
a)
y
x
z
MB
MT
Global and local thresholding
• Chromocenter Parameters
• Nuclear Topology Features

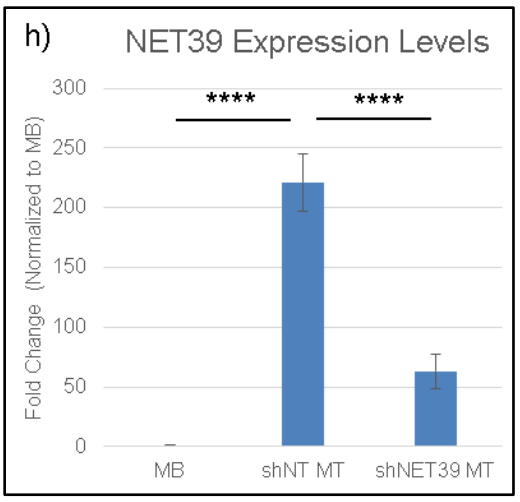
h)
NET39 Expression Levels
Fold Change (Normalized to MB)
300
250
200
150
100
50
0
****
****
MB
shNT MT
shNET39 MT

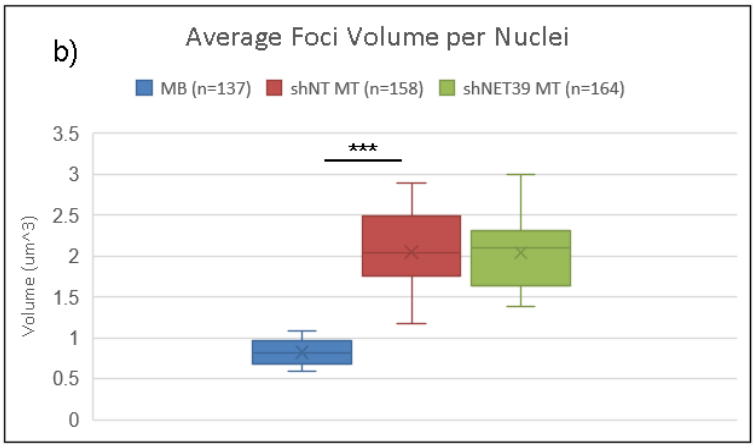
b)
Average Foci Volume per Nuclei
MB (n=137)
shNT MT (n=158)
shNET39 MT (n=164)
Volume (um^3)
3.5
3
2.5
2
1.5
1
0.5
0
***

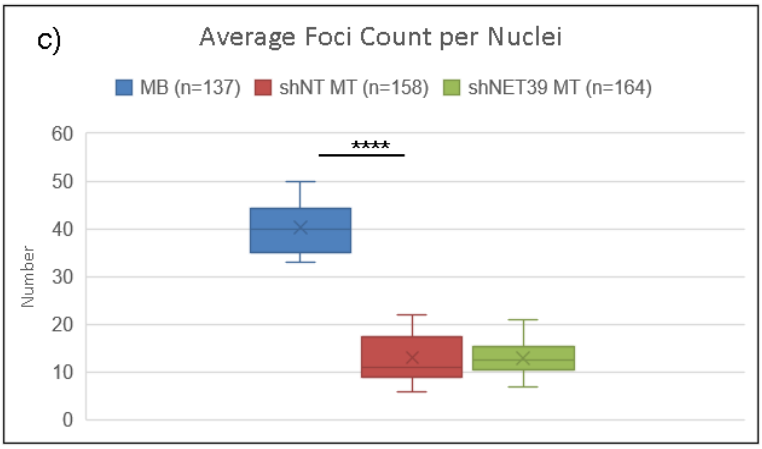
c)
Average Foci Count per Nuclei
MB (n=137)
shNT MT (n=158)
shNET39 MT (n=164)
Number
60
50
40
30
20
10
0
****

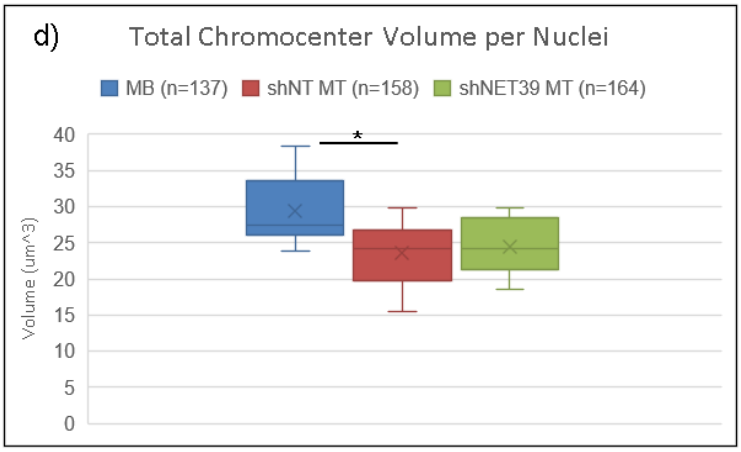
d)
Total Chromocenter Volume per Nuclei
MB (n=137)
shNT MT (n=158)
shNET39 MT (n=164)
Volume (um^3)
40
35
30
25
20
15
10
5
0
*

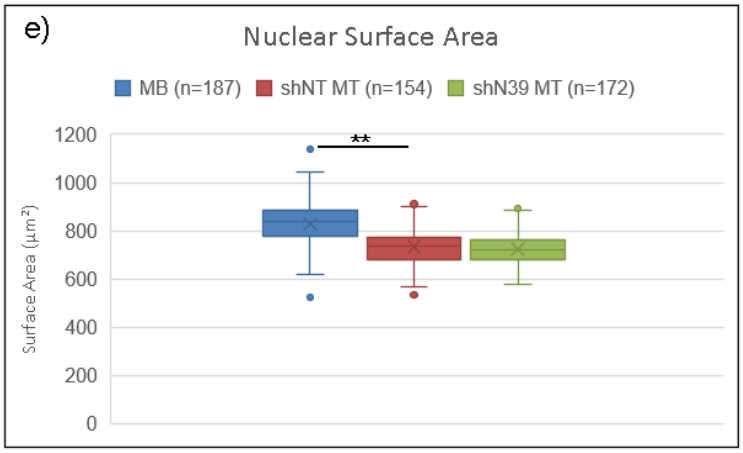
e)
Nuclear Surface Area
MB (n=187)
shNT MT (n=154)
shN39 MT (n=172)
Surface Area (µm²)
1200
1000
800
600
400
200
0
**

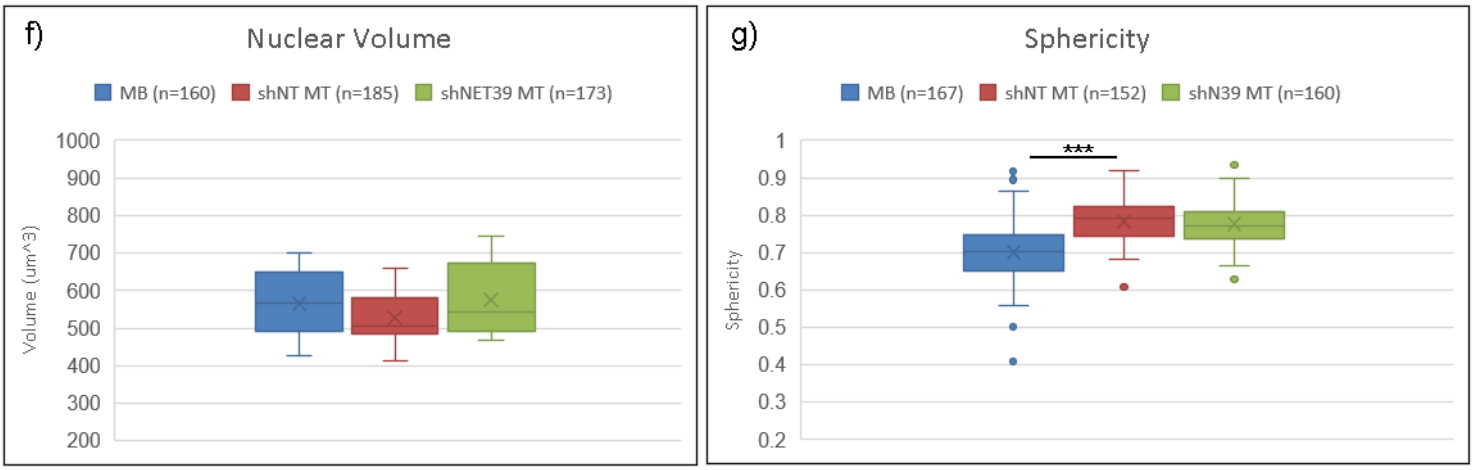

Fig 19) Box and whisker plot quantification of Chromocenter features and Nuclear Topology in MB, shNT MT and shNET39 MT nuclei. **a)** Schematic representing analysis workflow; **b)** Average Foci Volume per nuclei; **c)** Average Foci Count per nuclei; **d)** Total Chromocenter Volume per nuclei; **e)** Nuclear Surface Area; **f)** Nuclear Volume and **g)** Sphericity. One-way Anova followed by Tukey's HSD was used for statistical tests (*=p<0.05, **=p<0.01, ***=p<0.005, ****=p<0.0001). Pairs that only differ significantly are shown while non-significant pairs are not shown. **h)** qPCR verification of NET39 expression levels in MB, shNT MT and shNET39 MT (Error bars represent SEM). Data pooled from 2 Biological replicates for all experiments.

2.c) Does NET39 contribute to epigenetic reprogramming of repressed genes?

Analysis of our 'Interactome' datasets showed that repressive transcription factors and epigenetic enzymes form a major class of interactors for NET29 and NET39, some of which have been extensively studied and the molecular mechanisms by which they regulate genome organization have been fairly well dissected. Enzymes like Dnmt1 and Chd4 which appear as NET39 interactors have been shown to regulate deposition of DNA methylation and removal of histone acetylation respectively, both of which lead to gene repression in contexts spanning development and disease. (O'Shaughnessy-Kirwan et al., 2015), (Robertson et al., 2000). Since NET39 contributes to peripheral recruitment to repress anti-myogenic genes, we hypothesized that NET39 exploits interactions with repressive epigenetic modifiers to enforce transcriptional repression.

In order to understand epigenetic changes at a single gene loci level, we attempted to develop an imaging-based approach. Previous studies from the lab had used similar approaches by co-immunostaining for LacO locus (under the spatial control of an NE tether) and repressive histone modifications which allowed quantification of signal overlap and consequently presence of epigenetic mark on the locus. The motivation for developing such an approach stemmed from the fact that population averaged studies (like ChIP) tend to lose out on information like allelic exclusion and intrinsic single cell variability. It's often observed by Fluorescent in Situ Hybridization (FISH) that only a subset of all copies of the gene reposition in response to a stimuli. An example includes the IL2 locus in T-cell activation, where only one locus appears to reposition to the nuclear interior concomitant with T-cell activation (unpublished data), hinting at allele-specific spatio-temporal regulation. Further, in tetraploid systems like C2C12, averaging epigenetic profiles over 4 copies of gene loci may result in poorer approximation of the variability. Most importantly, this study would have facilitated studying temporality in genome organization .ie. do deposition of epigenetic marks precede/facilitate relocalization to the nuclear periphery or vice versa. Recent studies have used imaging-based approaches to identify nanodomains within chromatin marked by specific histone marks (Xu et al., 2018).

By combining Immunostaining for repressive histone marks (H3K9Me3, H3K27Me3) with Fluorescent in Situ Hybridization (FISH) for gene loci that reposition during myogenesis, we wanted to quantify density of epigenetic staining signal around labelled gene loci. Initially, the repressive chromatin landscape was analyzed by Immunostaining for H3K9Me3 and H3K27Me3 in MBs and MTs. Initial attempts at staining MTs proved to be unsuccessful. Most Immunostaining studies performed on MTs have achieved successful staining of cytoplasmic proteins using regular Immunofluorescence protocols. However, to improve nuclear staining, permeabilization conditions had to be optimized. By adopting a harsher permeabilization (15 minutes RT 1% Triton X-100) combined with a controlled Proteinase K treatment (30 seconds, 20 ug/ml), antibody accessibility was greatly improved. In order to improve signal to noise ratio, Airyscan

module of Confocal Imaging was employed. Airyscan module adopts the use of better detectors to bring down the x-y resolution to ~140 nm from ~240 nm for regular confocal microscopy.

Immunostaining revealed an interesting staining pattern for the repressive histone modifications. Specifically, H3K9Me3 is enriched in chromocenters and weakly stains the nuclear periphery, possibly constitutive heterochromatin (Fig 20b). Unexpectedly, H3K27Me3 is completely absent from chromocenters and stains two chromosome territory like bodies, possibly inactive X-chromosomes (Fig 20a).

a)

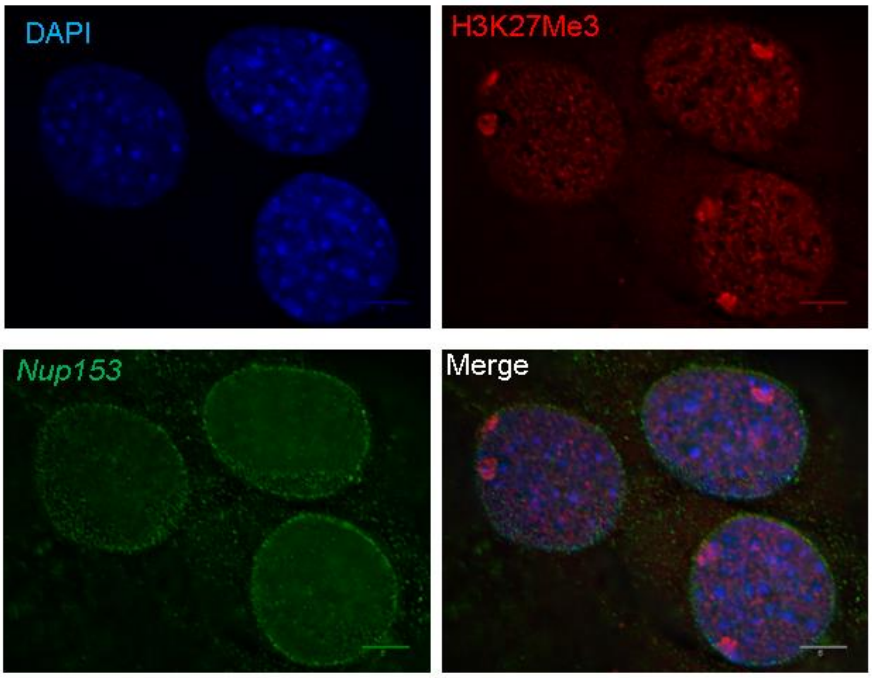

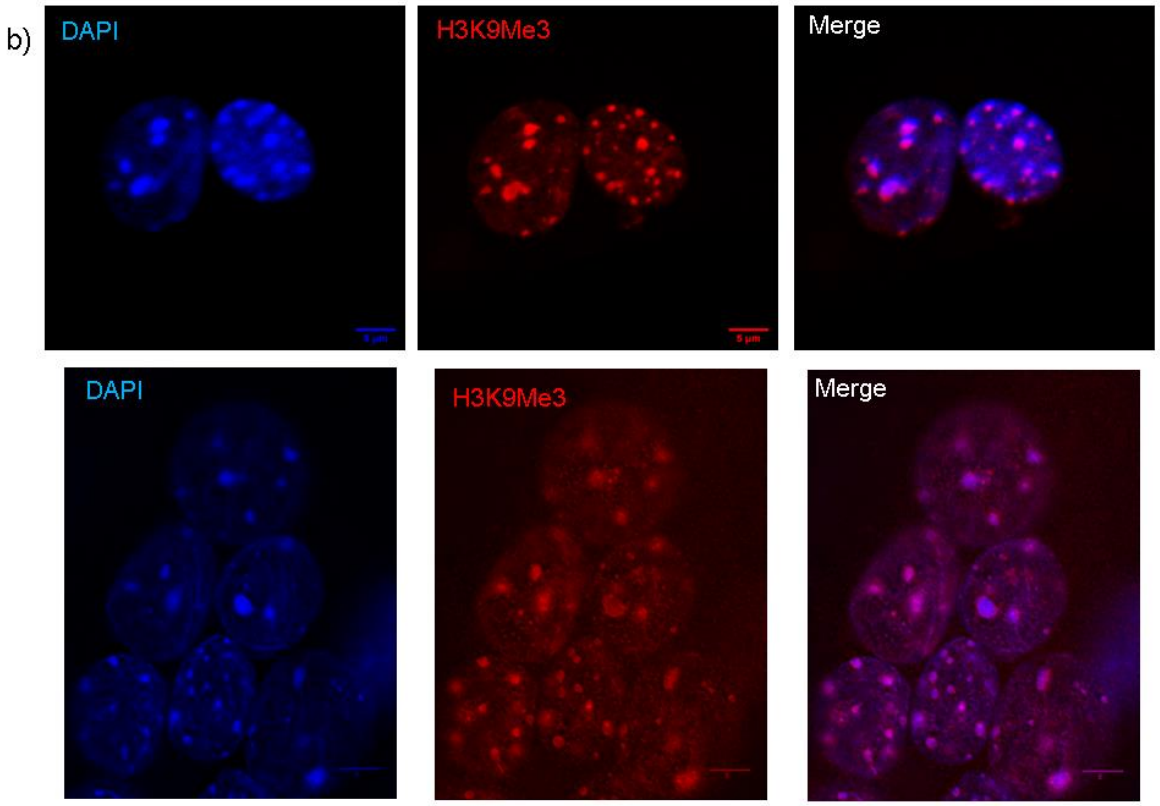

Fig 20) Representative images for repressive histone modification Immunofluorescence staining **a)** H3K27Me3 staining for MBs **b)** H3K9Me3 staining for MBs **(top)** and MTs **(bottom)** combined with High-resolution confocal Airyscan imaging

To label gene loci, different FISH approaches were adopted. Initial attempts using a 3D FISH approach which used milder fixation and permeabilization techniques to retain the 3D nuclear architecture proved to be completely unsuccessful in producing reasonable FISH signals (data not shown). Reasonable FISH signal was obtained by incorporating ethanol dehydration series and stronger denaturing conditions (Fig 21a). However, this resulted in a substantial loss of background H3K9Me3 staining. This protocol appeared to be even less efficient in MT. Adopting a 2D FISH protocol achieved great labelling of gene loci but completely altered immunostaining patterns. We decided to discontinue this approach and adopt a population-averaged ChIP-qPCR approach.

a)

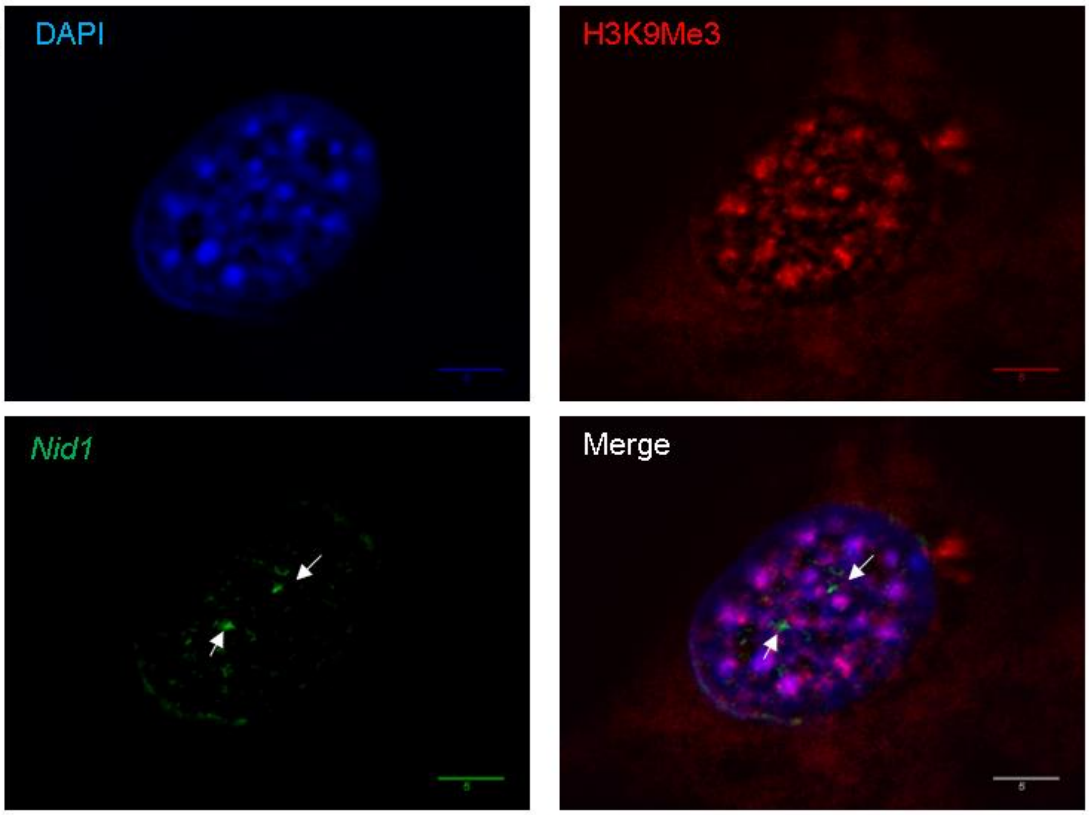

b)

	Fixation	Permeabilization	Observation
3D FISH	4% Formaldehyde – 10 mins	Liquid N_2 Freeze-Thaw; 0.5% Triton 5 mins	FISH signal completely absent, H3K9Me3 reasonably preserved
2D/3D Intermediate FISH	4% Formaldehyde – 10 mins	Ethanol Dehydration Series; 0.5% Triton 5-15 minutes; Proteinase K Treatment – 2 ug/ml – 30 seconds	Reasonable FISH signal in MBs but not MTs, significant loss of H3K9Me3 staining
2D FISH	3:1 Methanol:Acetic Acid on Isolated Nuclei	Ethanol Dehydration Series	Strong FISH signals for both MB and MT, severe loss of H3K9Me3 staining

Fig 21) a) Representative 2D/3D Intermediate FISH Image for *Nid1* gene loci immunostained with H3K9Me3. **b)** Summary of FISH conditions tested

To understand the extent of changes in histone modifications during myogenesis, published ChIP-seq datasets for available histone modifications were collected from GEO Accession servers and ChIP Peaks were visualized on IGV. Several genes which we previously found to get repressed and reposition to nuclear periphery during myogenesis in a NET39 dependent manner showed alterations in ChIP-Seq profiles between MBs and MTs from this publicly available data, generally losing activating histone modifications during myogenesis (Fig 22).

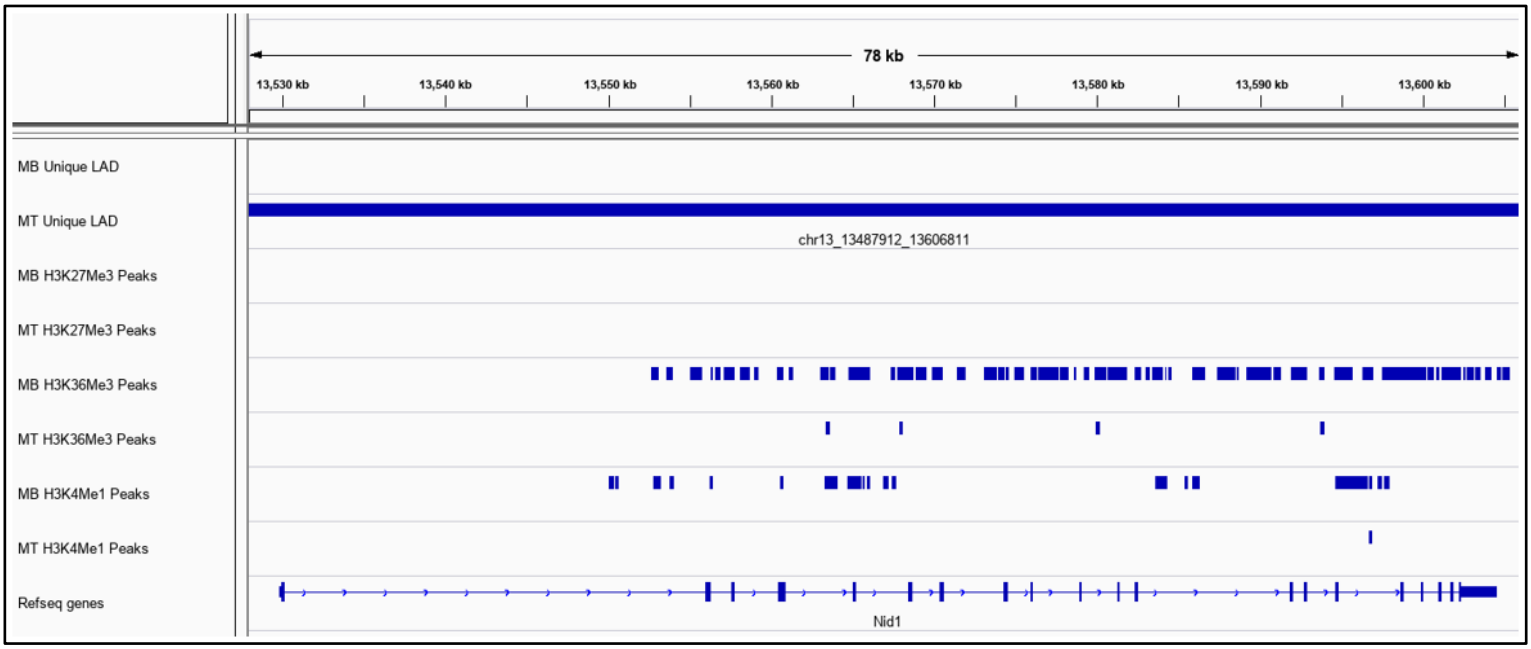

Fig 22) IGV track depicting changes in various histone modification peaks during myogenesis for *Nid1* gene. ChIP-seq peaks are shown for H3K27Me3 (repressive histone mark), H3K36Me3 (active transcriptional elongation mark) and H3K4Me1 (active histone mark) obtained from publicly available databases.

A ChIP-qPCR approach was adopted to address if *Nid1* and *Efna5* genes, which reposition to the NE and get transcriptionally silenced in a NET39 dependent manner during myogenesis (Robson 2015), also acquire H3K9Me3 histone modification in a NET39 dependent manner.

Primers directed against Ankrd1 enhancer (Decreased H3K9Me3 during myogenesis (Beyer et al., 2016)) and DHFR promoter (Increased H3K9Me3 during myogenesis

(Gurtner et al., 2008)) served as a pulldown and differentiation positive control. GAPDH promoter served as a negative control. Further, IgG controls were included to account for nonspecific chromatin pulldown. ChIP-qPCR was performed in MBs, shNT MT and shNET39 MT for different regions of *Nid1* and *Efna5* genes.

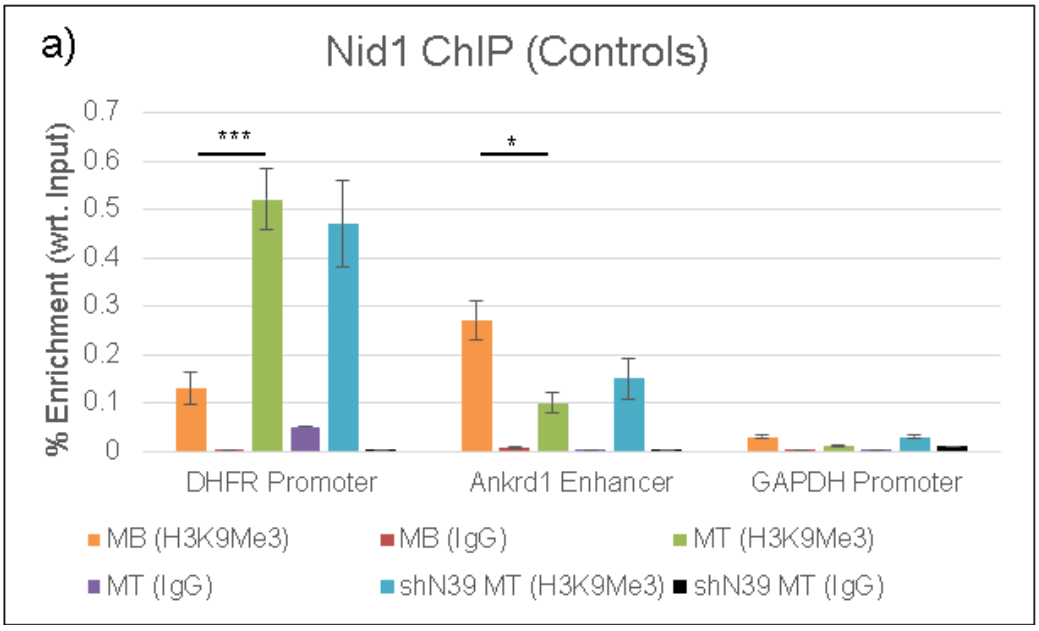

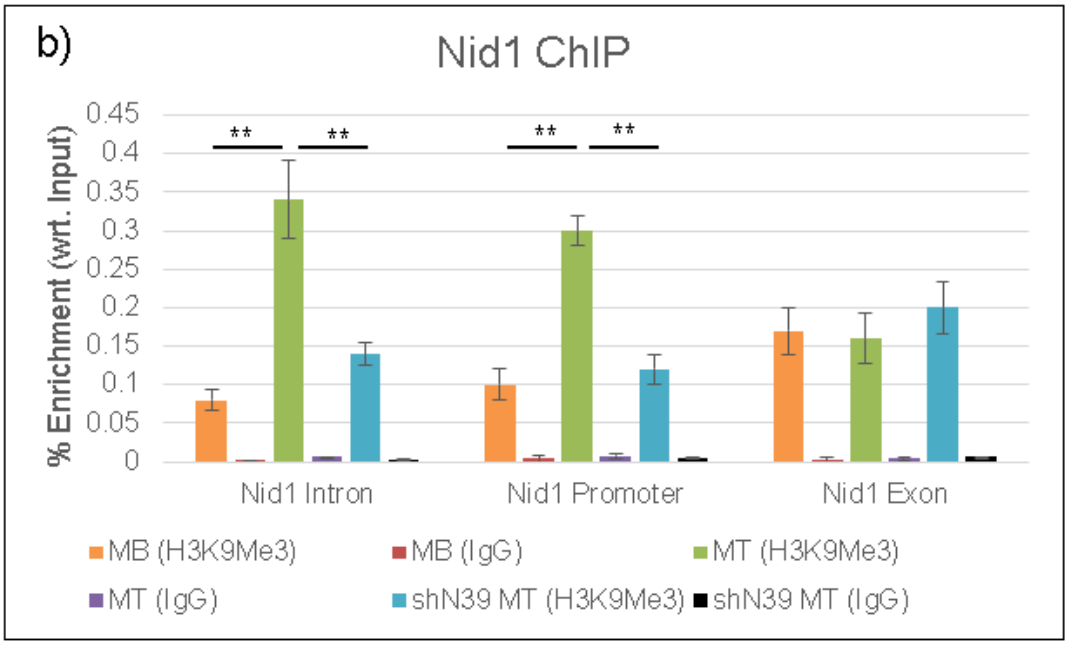

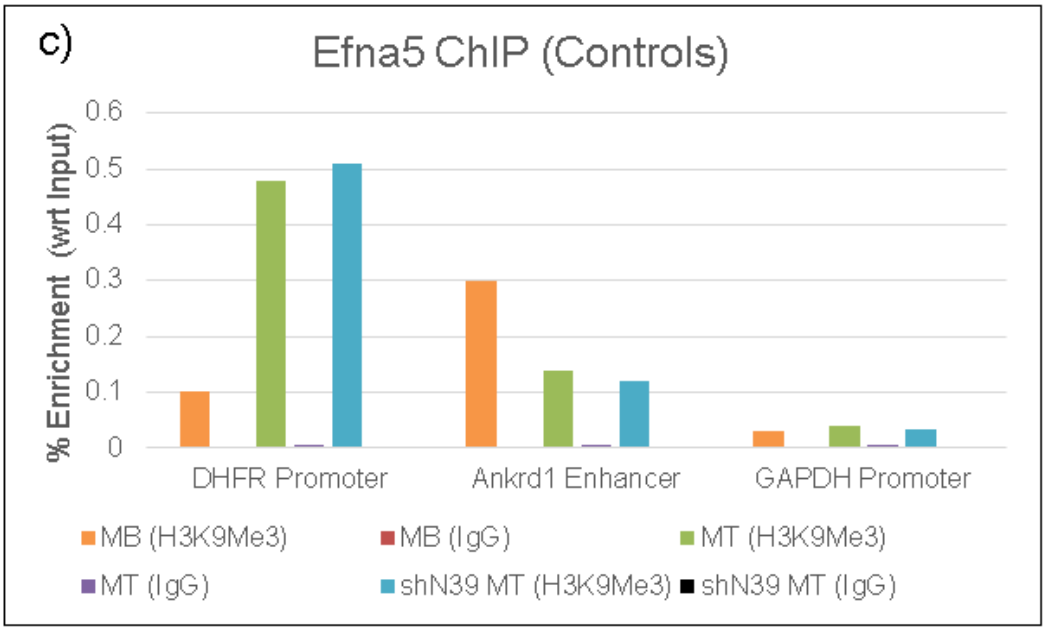
c)
Efna5 ChIP (Controls)
% Enrichment (wrt Input)
0.6
0.5
0.4
0.3
0.2
0.1
0
DHFR Promoter
Ankrd1 Enhancer
GAPDH Promoter
MB (H3K9Me3)
MB (IgG)
MT (H3K9Me3)
MT (IgG)
shN39 MT (H3K9Me3)
shN39 MT (IgG)

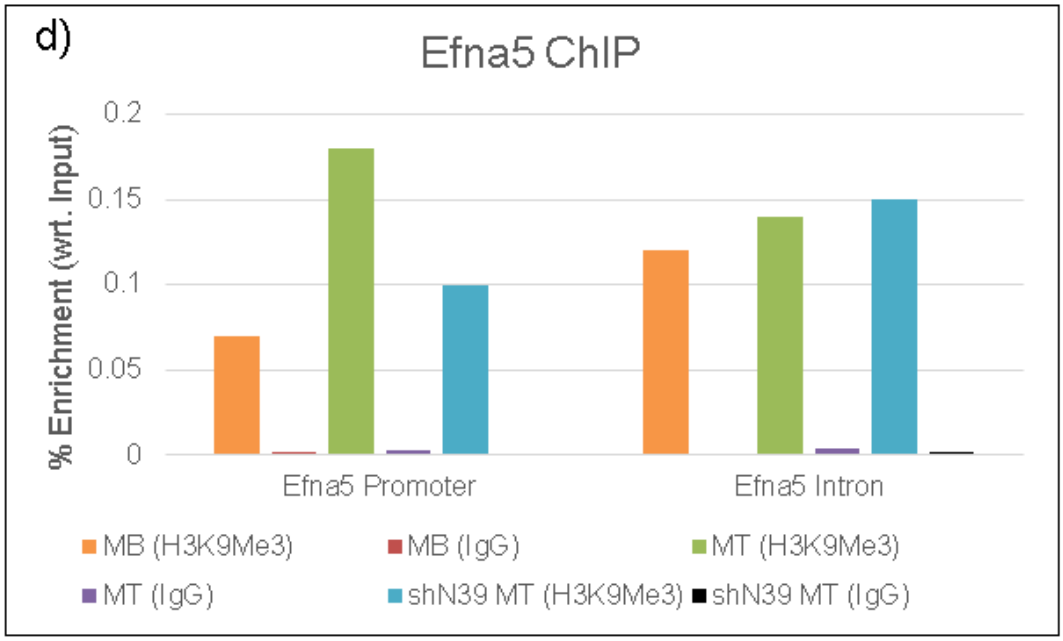
d)
Efna5 ChIP
% Enrichment (wrt. Input)
0.2
0.15
0.1
0.05
0
Efna5 Promoter
Efna5 Intron
MB (H3K9Me3)
MB (IgG)
MT (H3K9Me3)
MT (IgG)
shN39 MT (H3K9Me3)
shN39 MT (IgG)

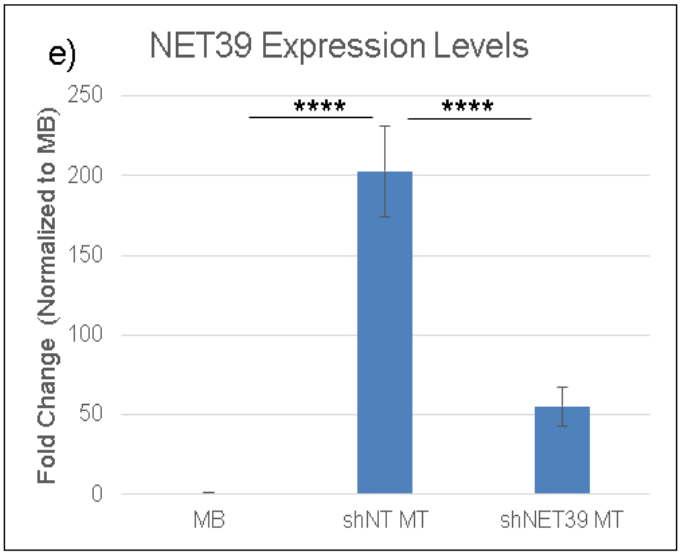

Fig 23) ChIP-qPCR analysis for H3K9Me3 occupancy on Nid1 and Efna5 genes. H3K9Me3 ChIP for **a,c)** Positive control regions DHFR Promoter and Ankrd1 Enhancer ; negative control region GAPDH promoter. **b)** Nid1 Promoter, Intron and Exonic regions (N=3) and **d)** Efna5 Promoter and Intron regions (N=1). Normalization was performed wrt 1% input. Two-way Anova was used to test significance between MB, control MT and shNET39 MT for IgG and H3K9Me3 pulldown conditions. Pairs that differ significantly (identified by Tukey HSD) are marked using '*****' (***=p<0.001, **=p<0.01, *=p<0.05) while non-significant pairs are not marked. H3K9Me3 pulldowns for all regions differed significantly from corresponding IgG. Error bars represent SDM. **e)** qPCR verification of NET39 expression levels in MB, MT and shNET39 MT (N=2). Error bars represent SDM.

Results indicate that both *Nid1* and *Efna5* promoters show a significantly increased H3K9Me3 deposition in shNT MT compared to MB (Fig 23 b,d). *Nid1* Intronic region also showed a significant increase while other tested regions didn't show a change (Fig 23 b,d). Further, H3K9Me3 deposition occurs in a NET39 dependent manner, evident from significantly reduced H3K9Me3 levels in shNET39 MT compared to shNT MT (Fig 23 b,d).

2.d) Does NET39 regulate features of the LINC complex?

During myogenesis, proliferating MBs fuse into a contiguous structure with aligned nuclei. There is a dynamic reorganization of cytoskeletal elements and adhesion factors to facilitate morphogenesis, resulting in massive changes in mechanical forces (Happe and Engler, 2016). These physical changes have important consequences in modulating genome organization. The Linker of Nucleoskeleton and Cytoskeleton (LINC) complex is the major mechanotransduction complex embedded in the NE which relays extracellular mechanical information into the nucleus to directly affect nuclear architecture (Pradhan et al., 2018). The LINC complex has been previously shown to regulate major aspects of MT fusion, branching and nuclei positioning (Bouzid et al., 2019) while mutations in LINC complexes can give rise to muscle-specific disease phenotypes (Meinke et al., 2014)

NET39 deficient MT (shNET39 MT) show interesting defects in overall shape and fusion characteristics. Compared to control MT (shNT MT), shNET39 MT are thicker, shorter and are often bent/curved (Fig 24a, regions depicted by yellow arrows). Also, shNET39 MTs show a branching phenotype where several MTs stem from a larger one. Further, NET39 is also known to regulate expression of proteins with known cytoskeletal functions. Since NET39 knockdown MT phenotypically resemble LINC mutant MT, we hypothesized that defective MT characteristics and altered genome organization patterns in shNET39 MT are via changes at the LINC complex. Most LINC complex proteins do not appear as significant interactors in our NET39 BioID dataset, suggesting that NET39 might not be directly involved in the assembly or anchoring of the LINC complex. So we reasoned that if NET39 potentially affected the LINC complex, it would have to be due to its function in fine-tuning of transcriptional regulation. Microarray analysis of expression of LINC complex proteins showed that there is a significant change in the transcriptional profile of several LINC complex proteins upon myogenic differentiation (Fig 24b). To understand if NET39 regulates LINC complex proteins' expression, we tested the expression of a subset of these LINC complex proteins in shNET39 MT by qRT-PCR. Results indicated that most LINC complex proteins do not show altered expression in shNET39 MT compared to shNT MT (Fig 24c), suggesting

that NET39 does not exert transcriptional control over LINC complex at least for the isoforms and components tested.

a)

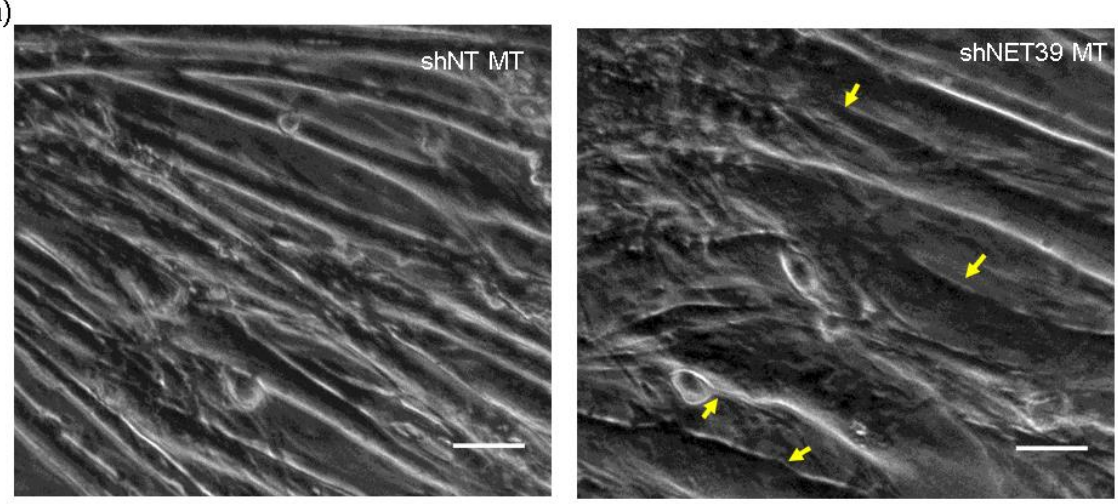

b)

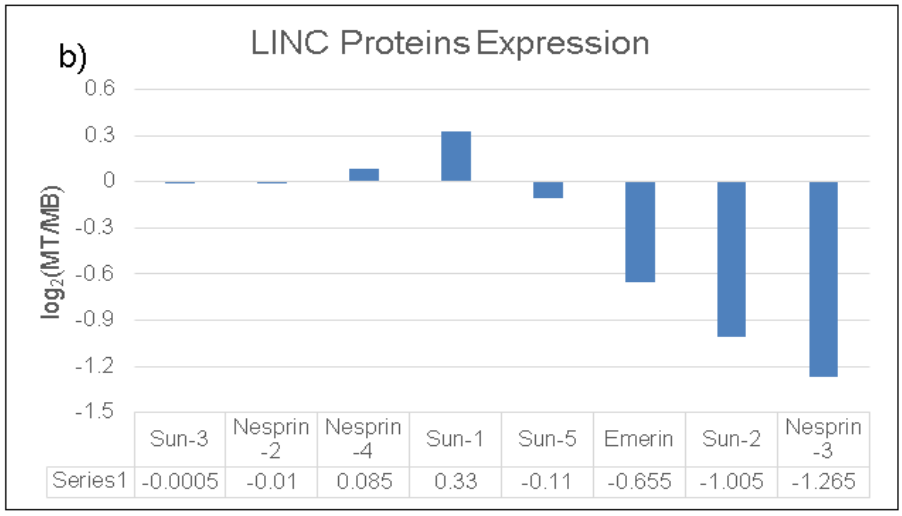

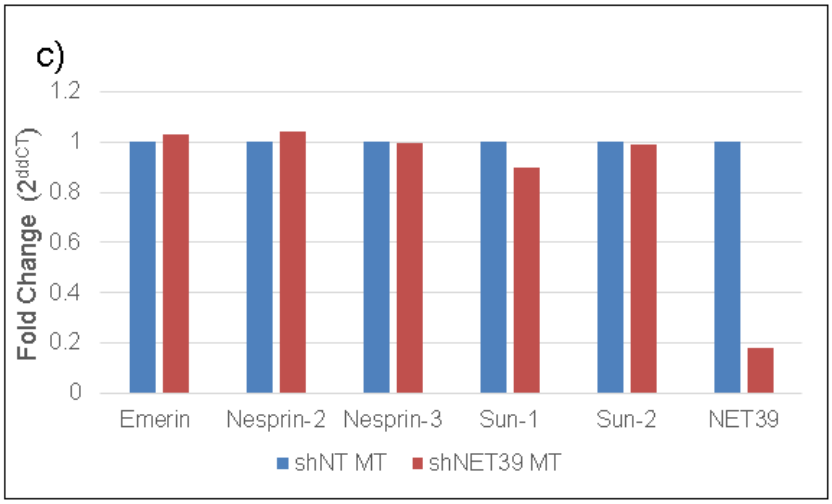

Fig 24) Role of NET39 in modulating LINC complex. **a)** Phase contrast microscopy images of shNET39 MT and shNT MT show morphogenesis defects of shNET39 MT. Scale bar represents 50 microns, **b)** Microarray analysis of expression profiles of LINC complex proteins during myogenesis. **c)** qPCR Analysis of selected LINC complex proteins and NET39 in shNT MT and shNET39 MT (N=1)

3) Reversibility in genome organization

An important open question in the field of genome organization is the extent of reversibility of genome organization changes, particularly due to experimental difficulties to characterize reversibility in systems. To understand if genome organization changes that occur during myogenesis is reversible, we attempted to develop a tissue culture model of muscle injury using a peptide toxin approach. Several studies have shown that inducing muscle injury in mice leads to upregulation of muscle repressed genes like *Efna5, Cxcl1* and *Ptn* in injured tissues (Caruelle et al., 2004; De Paepe et al., 2012; Stark et al., 2011) . However, these experiments have been done on whole tissue extracts which are highly heterogeneous. Thus, it is currently unclear if the observed increase in transcripts are due to reactivation in injured muscle fibers or from newly proliferating satellite stem cells. Our C2C12 system provides a less complicated system to test these questions. Literature survey of Notexin studies showed that muscle damage experiments have previously never been reported in a tissue-culture system,

suggesting that we would have to adopt a blind-folded approach to standardize Notexin mediated muscle damage in C2C12 system. Further, the only documented mechanism of Notexin mediated muscle injury showed that Notexin acted at the level of neurotransmitter acetylcholine release by affecting synaptic vesicle formation and synaptosome assembly in pre-synaptic junctions. These receptors are absent in C2C12s, but nevertheless provided a system to explore other mechanisms/pathways that Notexin can affect.(Cull-Candy et al., 1976)

For Notexin mediated muscle injury in mice, Notexin was directly injected into muscle at a concentration of 10 ug/ml and followed for several weeks. For our initial attempts, we used Notexin at 2.5 ug/ml for 24 hours on MTs. Phase contrast microscopy on Notexin treated MT showed that several larger MTs detach and form clumps (Fig 25a, regions highlighted by yellow arrows). No free-floating cells or cell debris was observed.

qPCR results suggest that anti-myogenic genes *Efna5* and *Cxcl1* which are repressed in MTs get reactivated upon muscle injury, although the extent of reactivation appears to be variable across replicates, especially for *Ptn* (Fig 25b). Interestingly, this reactivation is coupled with a slight reduction in NET39 transcript levels, suggesting that loss of NET39 might enable the activation.

a)

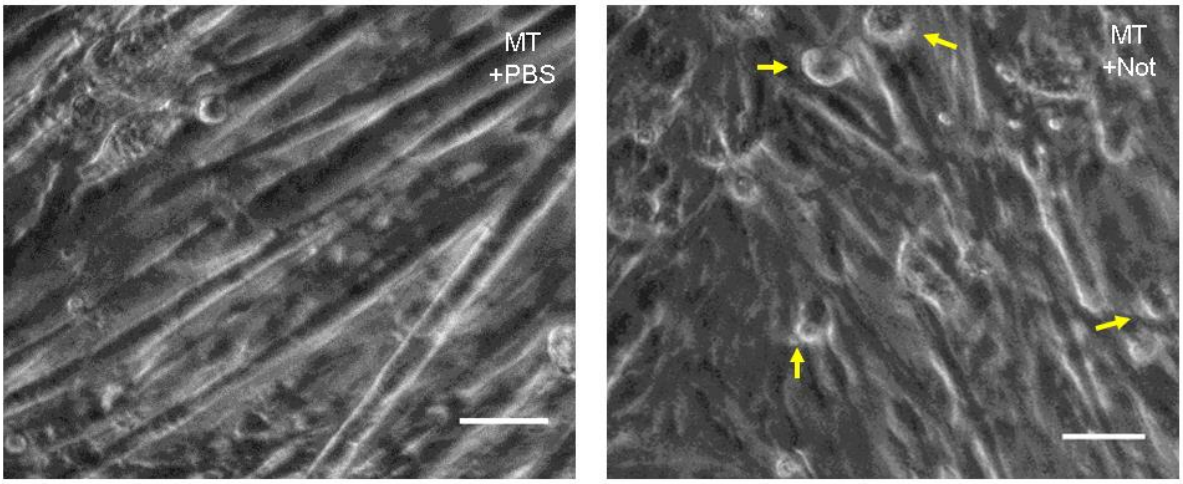

b)

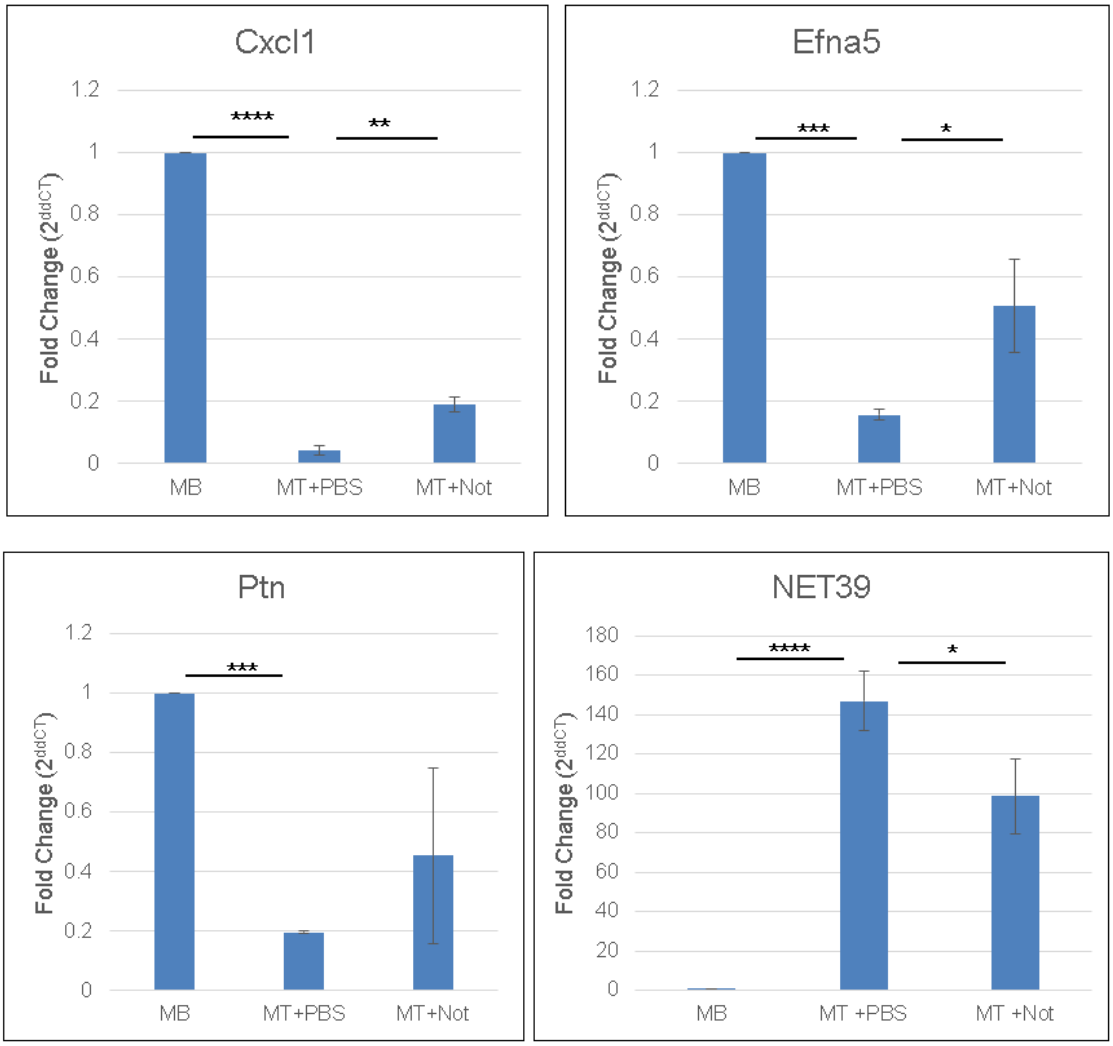

Fig 25) a) Phase contrast microscopy representative images of PBS and Notexin (Not) Treated MT to show defects in MT organization upon muscle injury. Scale bar represents 50 microns. **b)** qPCR expression profiles of Cxcl1, Efna5, Ptn and Ppadc3 (NET39) genes in MB, PBS treated MT and Notexin treated MT. Error bars represent SDM. Data from 3 biological replicates for *Cxcl1, Efna5* and *Ptn*. Data from 2 biological replicates for NET39. One-way Anova followed by Tukey's HSD was used to test for significance (*=p<0.05, **=p<0.01, ***=p<0.005, ****=p<0.001). Only pairs that differ significantly are marked using '*'.

To address the possibility that this reactivation is coupled with release of genes localized at the nuclear periphery, we analyzed spatial positions of these genes with

respect to the nuclear periphery (marked by DAPI edge) using 2D FISH (Fig 26a). Results indicate that *Efna5, Ptn* and *Cxcl1* genes move significantly towards the nuclear periphery during myogenesis (Fig 26b). Further, upon Notexin treatment, *Efna5* relocalizes slightly but significantly into the nuclear interior while other genes do not show the same effect, although a slight shift in interquartile range towards nuclear interior can be observed for *Cxcl1*. (Fig 26b)

a)

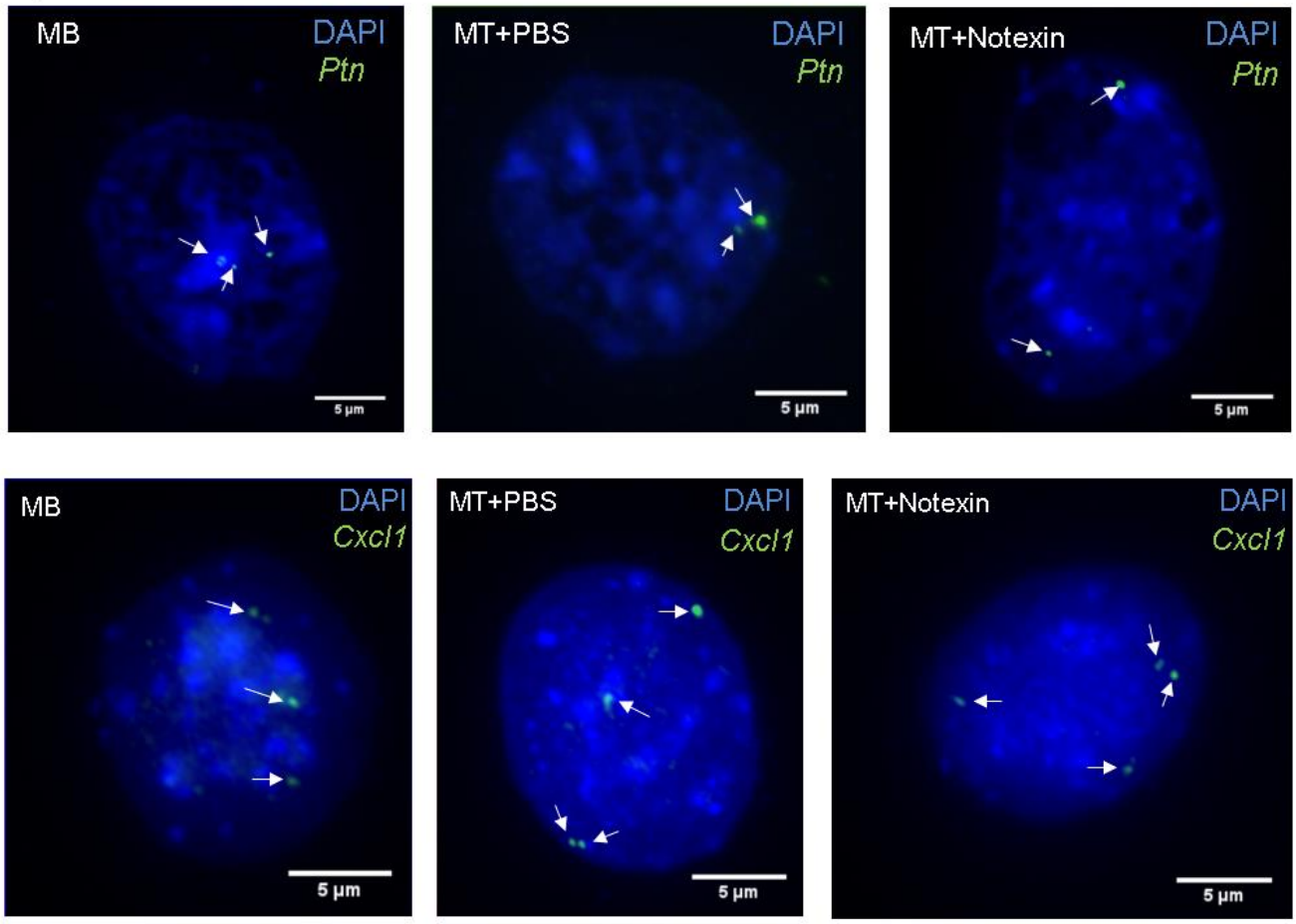

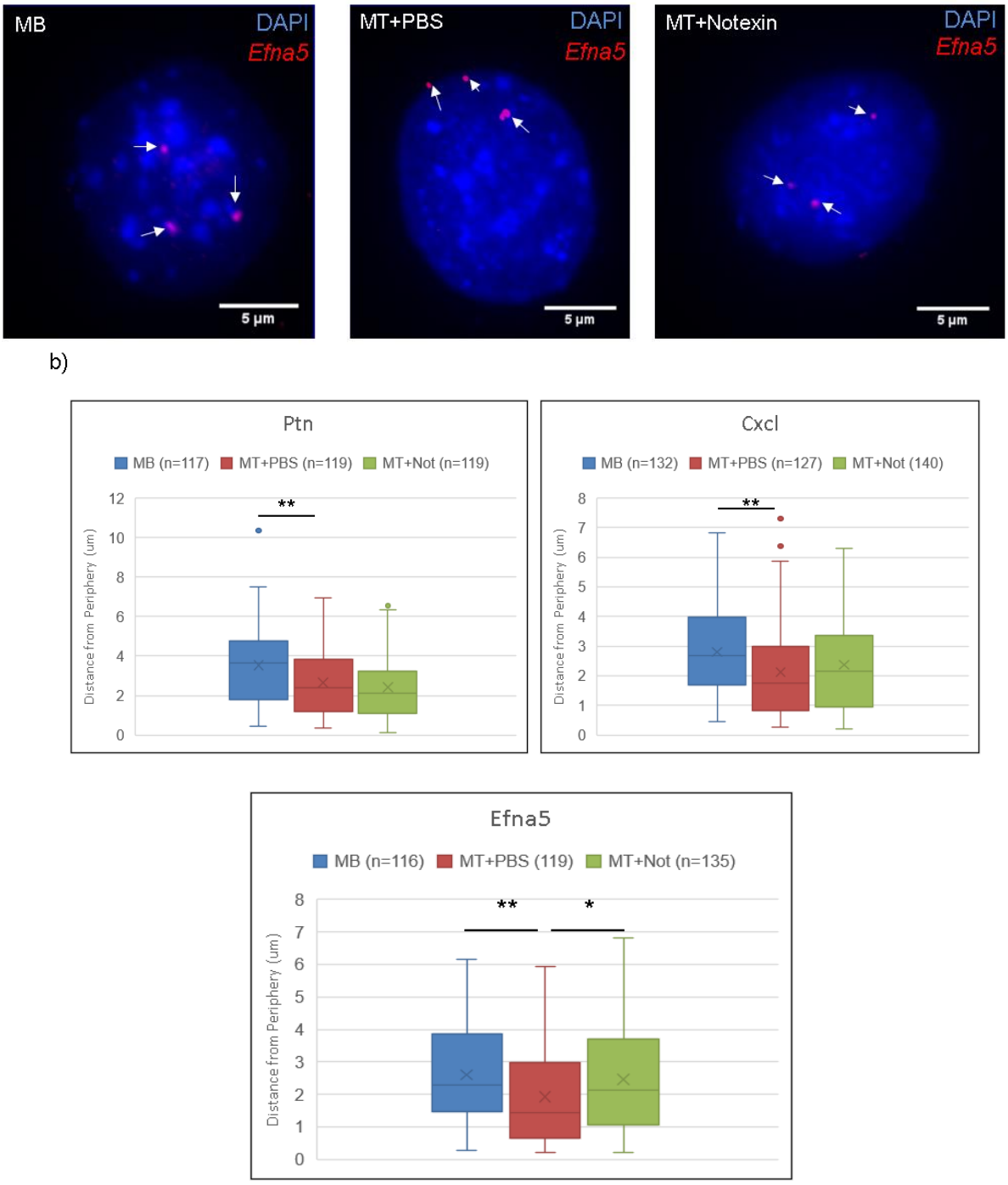

Fig 26) 2D FISH for MB, PBS treated MT and Notexin treated MT. **a)** Representative panels of FISH images for *Ptn, Cxcl1* and *Efna5* gene loci. **b)** Box and whisker plots for quantification of nearest distance from periphery for *Ptn, Cxcl1* and *Efna5* gene loci. One-way Anova followed by Tukey's HSD was used to test for significance (**=p<0.01, *=p<0.05). Pairs that don't differ significantly are not marked. Data from 1 Biological replicate.

In an ideally differentiated sample with high myogenic index, non-proliferating MB (NP-MB) form a small but significant fraction of the population and lie as a monolayer beneath MTs, suggesting the possibility that the observed augmented transcription could be from either population. These NP-MB do not immunostain for myogenic markers like Myh1 and are transcriptionally similar to proliferating MB, although studies have not systematically investigated differences between them. To test which fraction of the population contributed to the observed increase in transcription, we then isolated MTs from non-proliferating MBs by controlled trypsinization and further enriched intact MTs by limited centrifugation. The fraction of MTs enriched from Notexin treated samples was significantly lesser than control MTs, as observed by visualizing an aliquot under the microscope. Also, the total RNA yield obtained from enriched Notexin treated MTs was only a tenth of the control MT RNA yield. These observations suggest that larger MTs likely break up as a consequence of the Notexin treatment and fail to get enriched. qPCR analysis of the isolated populations reveals that the both non proliferating MBs and MTs show increased transcription in response to Notexin, although MTs contributed only marginally while non proliferating MBs appeared to respond more dominantly with several fold increase in transcript levels. (Fig 27). Interestingly, all genes appeared to respond strongly to the Notexin treatment. However, further replicates are needed to corroborate these observations.

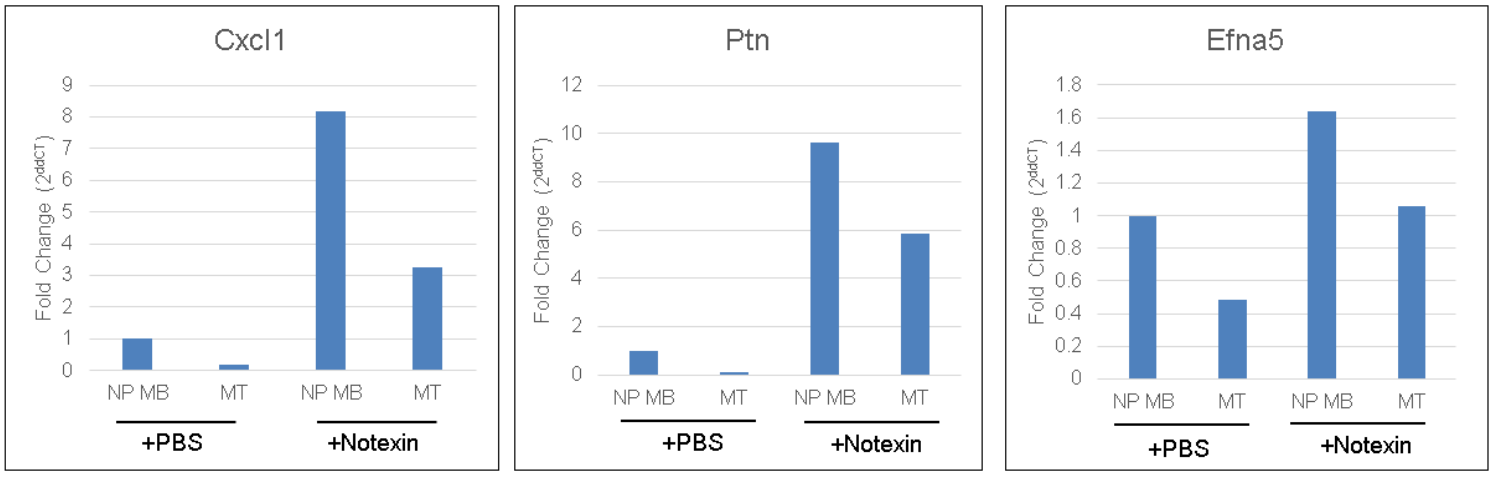

Fig 27) qPCR analysis of expression profiles of non-proliferating MB (NP-MB), isolated MT (MT) in PBS and Notexin treated conditions. Data from 1 Biological Replicate.

Discussion and future directions:

In this study, we attempted to understand the functional interplay between the NE and genome organization in myogenesis. Previous studies from the lab used a moving window of 100 Kbp to identify regions which reposition with respect to the NE with significant changes in average DamID scores. This approach reflects large scale changes (representing regions of ~500 kb) which allows identification of statistically significant relocalizations and was commonly used by studies a few years ago. However, though several papers have reported LAD sizes of up to 1 Mbp, more recent studies have suggested that LADs typically vary in size from 20-100 Kbp (average of ~30 Kbp) and are thus much smaller than the window previously analyzed, necessitating the need to use smaller genomic windows. We believed that this approach might help in identification of additional NE associated genomic regions with novel uncharacterized genes and regulatory elements. However, the obvious drawback in this approach is sequencing noise and statistical verification leading to the possibility that a fraction of LADs (and consequently genes under the regulation of those LADs) are artifactual.

Like previous studies, our analysis suggests that genes important for myogenesis are under regulation of LADs. However, my study expanded the list of genes which dynamically reorganize with respect to the nuclear periphery but also showed that these genes are mostly unrelated to myogenesis. These results suggest that a significant fraction of genes that reposition during myogenesis i.e. which are associated with so-called ‘ghost’ LADs and have no studied function in myogenesis, are unlikely to affect myogenesis directly as they do not show any transcriptional change. These observations could be explained by three different but not necessarily mutually exclusive possibilities.

1) Genes which are important for myogenesis tend to reposition as larger units (which are reliably identified by Differential Region analysis), possibly driven by transcription activators or repressors, while other unrelated genes belonging to the local cluster show altered LAD status as a consequence of this. In principle, one can test this hypothesis

by analyzing the genomic distance of these ‘ghost’ LADs in reference to pro- and anti-myogenic repositioning genes.

2) Our preliminary analysis of the additionally identified genes suggests that microRNAs and long-noncoding RNAs are under LAD regulation. These regulatory RNAs are often much smaller than protein coding genes and are thus under the control of smaller LADs. It is important to recognize that DamID maps are probabilistic and represent population variability. For instance, a recent study in the adipogenesis system has shown that adipose derived secreted miRNAs regulate gene expression in other tissues (Thomou et al., 2017) and further these miRNAs are under control of LADs (Schirmer lab, unpublished). In this case, it is possible that release of miRNA encoding regions (coupled with activation) from LADs in a subset of adipocytes might prove sufficient to achieve its secretory functions for entire tissue, further reinforcing the idea that intrinsic variability must be considered in a context dependent manner. Our current preliminary study should be extended to verify if regulatory RNAs change in expression (using specific qPCR methods) and spatial positioning (using FISH) in our myogenesis system. Further, enhancer elements were also identified by my analysis, further reinforcing that regulatory elements are under the control of ‘ghost’ LADs. To further dissect how LADs regulate enhancers, released enhancers can be probed for activity by testing for enhancerRNA transcription as well as their spatial positions with respect to target genes using FISH.

3) Another interesting explanation is that these ‘ghost’ LADs serve as anchors to potentially facilitate distal chromatin looping and internal chromatin compartment assembly, thereby indirectly affecting myogenesis related processes. A recent study in the Lymphocyte system has provided evidence for a related hypothesis showing that LADs might facilitate enhancer-gene associations by constraining their 3D diffusion search space (Robson et al., 2017). An interesting future direction would be to systematically perturb LADs and/or inter LAD regions using CRISPR to alter loop lengths and then investigate effects on internal chromatin compartment assembly.

We performed correlative studies of Hi-C, DamID and microarray datasets to understand how NE regulates higher order genome organization. An interesting observation from genome-wide observation of the Hi-C datasets is that on average, MT genome shows a higher normalized contact frequency, which we thought was a consequence of chromatin compression. However, Hi-C normalization process involves a normalization term which uses the genome-wide average contact frequency for all genomic loci at a fixed genomic distance, which should theoretically account for changes in genome packing. Further, we also observed that compartments in MTs tended to be sharper and better defined which might potentially hint at better compartment insulation and reduced cis-trans interactions, but further quantification is required to establish this as a genome-wide phenomenon. For our Hi-C normalization, we used Iterative Correction and Eigenvector Decomposition (ICE) normalization method, which is known to be computationally efficient but has a few drawbacks such as weaker correlations between replicates at lower resolutions, quality of TAD calling etc. (Lyu et al., 2020) Thus, it might be beneficial to reanalyze our Hi-C datasets using other data normalization methods.

Our correlative studies between Hi-C and Microarray datasets show only a subset of genes that switch compartments also exhibit a change in transcription, suggesting that compartment switching does not necessarily imply change in transcriptional status. Further, we also observe that genes that switch from A to B compartment tend to gain LADs while genes that switch from B to A compartment tend to lose LADs. This is suggestive of the possibility that LADs help in maintenance of inactive B compartment. Alternatively, these correlations might be a consequence of transcription driving changes in both LAD and compartment status. Further, our GO Enrichment analysis of genes that switch compartments suggest that most pro- and anti-myogenic genes are already in A and B compartments respectively. This might be a consequence of the fact that MBs, which are lineage committed progenitors, have already ‘primed’ genomic contacts (and consequently do not need to switch compartments to interact with distal regions) which can facilitate rapid responses to differentiation cues. Further, these ‘primed’ genes may be transcriptionally fine-tuned by LADs potentially under the control

of muscle-specific NETs. Individual inspection of several genes which were already in the A compartment that lose LADs concomitant with transcriptional activation displayed increased eigenvalue scores (which are reflective of compartment strength) upon differentiation (Fig 28).

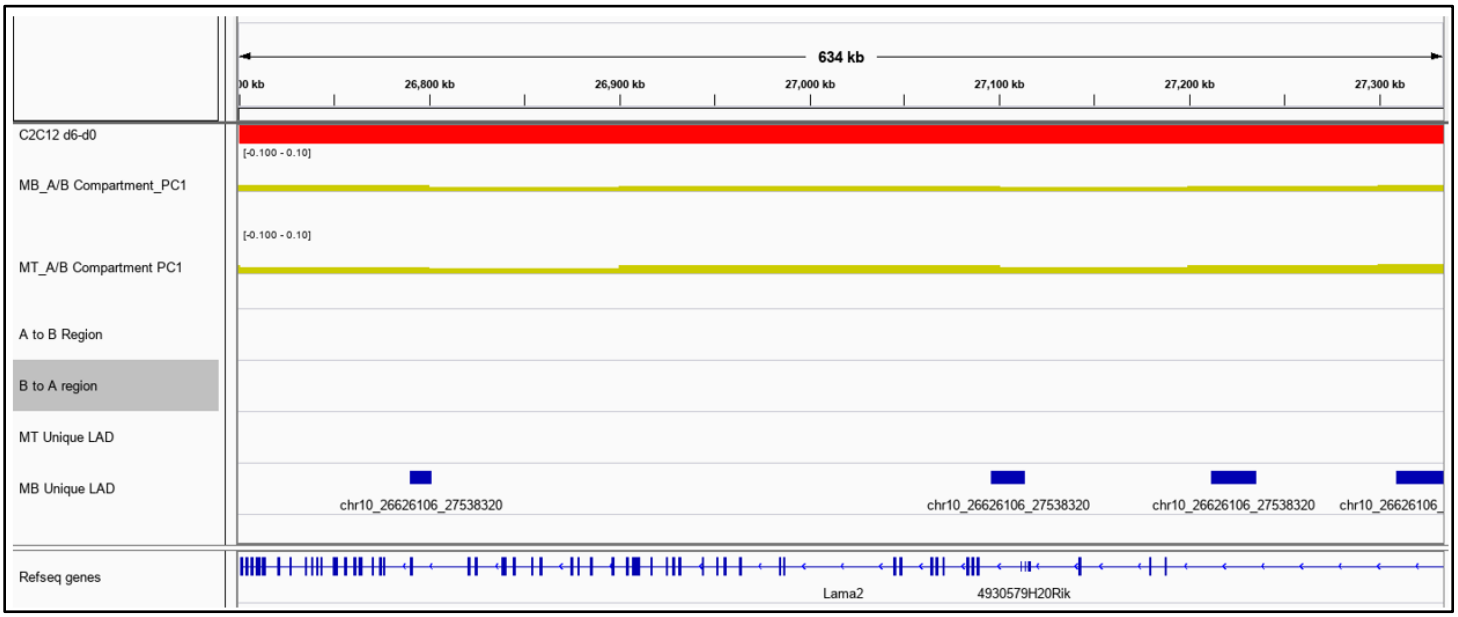

Fig 28) IGV track for pro-myogenic LAMA2 gene representing Microarray Expression data (log_2(MT/MB)), MB and MT Compartment PC1 values, A-B and B-A compartment switching regions, MB and MT unique LADs. **Key**-- Microarray Expression: Blue- Downregulated, Red- Upregulated; PC1 Compartment values: Yellow- Positive/A compartment, Pink- Negative/B compartment

One possible explanation for these genes is that they are under the regulation of bivalent promoters and are poised for transcriptional activation, suggested by a previous study in embryonic stem cells which showed that bivalent promoters favor a more A compartment structure (Mas et al., 2018). This also hints at a possibility that the nuclear envelope might regulate resolution of bivalent genes. Interestingly, expression analysis of various Histone Methyltransferases (HMTs), Histone Demethylases (HDMs), DNA Methyltransferases (DNMTs) and DNA Demethylases (TETs) which change significantly in expression upon differentiation shows that Epigenetic Writers (which regulate deposition of both repressive and activating histone marks) get significantly downregulated while Epigenetic Erasers (which regulate removal of both repressive and

activating histone marks) get significantly upregulated (Fig 29). This hints at a possibility that several pro-myogenic genes belong to bivalent chromatin in MBs and a global resolution of bivalency during myogenic differentiation. However, this preliminary study should be extended to systematically analyze correlations between DamID and ChIP-Seq datasets of H3K4Me3, H3K27Me3, stalled and elongating RNA Polymerase II to verify if loss of LADs correlates with loss of promoter bivalency.

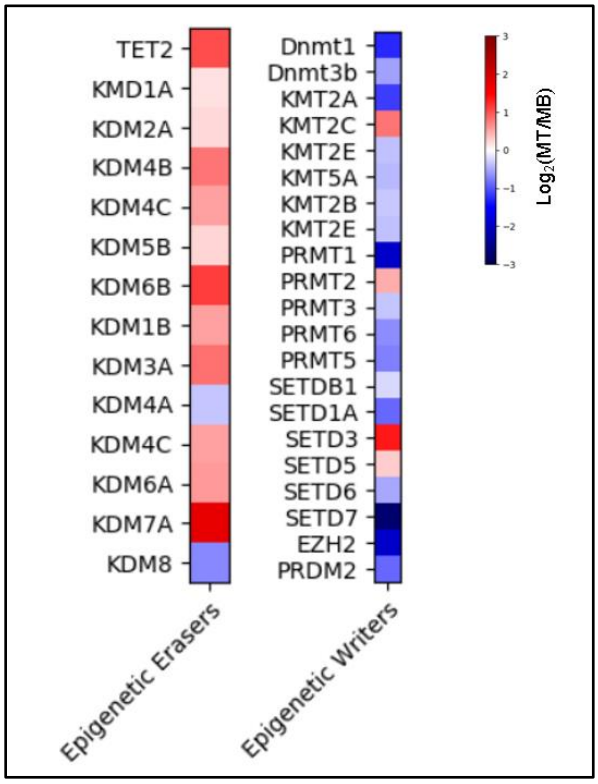

Fig 29) Heat map representing microarray expression profiles during myogenesis for two classes of genes, namely, Epigenetic Erasers and Epigenetic Writers. **Key**—Red: Upregulated; Blue: Downregulated

Our Hi-C datasets do not have enough read depth to further refine the A and B compartments; however, an earlier study in the lymphocyte cell line used roughly 100x sequencing depth to be able to further break the A and B compartments into A1,A2,B1,B2,B3 and B4 subcompartments (Rao et al., 2014). These subcompartments are characterized by fine differences in spatial profile, but interestingly were further found to correlate with distinctive epigenetic features. For instance, genes which

require transient activation get released from the B2/3 compartment at the nuclear periphery into the A2 compartment which is ~0.6 µm from the nuclear periphery (Robson et al., 2017). Our current Hi-C dataset/analysis methods might not be sensitive enough to identify this change and might erroneously classify A2 genes as belonging to the B compartment.

Several studies have investigated relationships between Hi-C datasets, histone ChIP-seq profiles , DNA methylation profiles, Chromatin Accessibility and replication timing(Rao et al., 2014),(Li et al., 2019),(Greenwald et al., 2019). However, functional interplay between LADs and chromatin compartment assembly remains underappreciated and poorly understood. Compartment switching is almost always studied in the contexts of transcriptional shutdown, loss of enhancer contacts etc. and rarely contrasted with spatial positioning with respect to the NE. Our results provide support for the view that LADs play a significant role in chromatin compartment maintenance and switching (Fig 16), although it is likely that more conventional gene regulatory mechanisms like transcription factor occupancy still dominates A/B compartment maintenance. A comprehensive study in the Lymphocyte system has uncovered how proximal and distal LADs potentially fine tune expression by regulating internal chromatin compartment (Robson et al., 2017). Computational approaches to model genome organization have suggested that strong lamina - heterochromatin attraction and intra- euchromatin interactions can explain spatial genome organization and reproduce experimentally obtained Hi-C patterns (Buckle et al., 2018; Falk et al., 2019).

NET39 mediated genome organization

Only in the last decade people have explored the diverse proteome of the NE. Most of these recently found NETs are poorly studied. Currently we do not have a reliable estimate of the number of NETs that have genome organizing functions; however, ten were found with such function out of roughly 50 screened, suggesting that there may be many NETs contributing to this function. Further, a large fraction of these NETs are not structurally characterized and in fact have a very wide range of either known functional

domains or domains of unknown function, thereby making it difficult for structure-based function inference. Recently, NET29 has been shown to be an ion channel with important roles in pain sensation (Beaulieu-Laroche et al., 2020), though at the same time it is reported to alter genome organization with the result of changing expression of a dozen different ion channels. Whether its contribution to ion channel function is direct and/or indirect, protein primary sequence-based domain prediction tools would never have identified NET29 as a potential ion channel nor as a chromatin- binding protein, thus highlighting the limitations of our current methodologies. Tissue specific epitope masking and NE targeting further adds another layer of complexity in studying tissue specific NETs. Further, the mechanisms by which these recently found NETs interact with chromatin is also not well understood. Liver-specific NET47, which is very similar to the ubiquitous NET LBR, has a chromo shadow domain which can bind chromatin. Interestingly, NET47 also has sterol dehydrogenase activity, suggesting that NETs can have multiple functions which may not be related to genome organization. NET5 has DNA binding domains and Zinc Finger motifs and therefore is likely to exert genome organization functions directly. However, this is not the case for NET29 and NET39 as they lack DNA binding domains. This necessitates the need for protein interaction partners or indirect mechanisms to explain their observed effects on genome organization.

We investigated several pathways by which we thought that NET39 can exert its genome organization functions. Specifically, we investigated if NET39 affected genome organization by regulation of i) LINC complex ii) chromocenter organization and nuclear topology and iii) repressive epigenetic features. Our results suggested that NET39 plays a minimal role in regulating the LINC complex and topological features on the nucleus in myogenesis, ruling these out as possible mechanisms by which NET39 affects myogenesis. To investigate if NET39 regulates epigenetic features of regions under its positional control, we attempted an imaging-based approach which had several technical difficulties, particularly related to denaturing conditions of FISH and permeabilization of MTs. One possible method to overcome the harsh conditions of FISH is to develop a CRISPR-Cas approach to target fluorescently labelled catalytically

dead Cas9 protein to our gene of interest (targeted by multiple guide RNAs) and couple that with immunofluorescence staining for epigenetic marks.

Our ChIP results lends support to the fact that NET39 helps in fine tuning of repression of critical genes during myogenesis. In absence of NET39, transcriptional repression is still observed but complete shutdown isn't achieved. This is suggestive of the possibility that the repressive histone modifiers which interact with NET39 possibly coordinate/complex with transcriptional repressors to help in enhanced repression of genes under the control of NET39 and serves to dampen stochasticity in transcriptional repression by adding another layer of regulation. Several genes that are under NET regulation like *Nid1, Cdk1* and *Efna5* are often needed early in myogenesis but are inhibitory to myogenesis in later stages. This suggests that muscle NETs aid in shutdown of genes that require tight regulation in a time-critical manner. Also, the nuclear periphery might serve as a region to concentrate the repressive factors and potentially sterically exclude transcriptional machinery, reinforcing transcriptional inactivation. However, several questions remain unanswered. Importantly, our ChIP study doesn't identify if deposition of repressive histone modifications (consequently modifying the transcriptional status of a gene) precedes peripheral recruitment or vice versa. Further, we also do not know if this repression is a general feature of the nuclear envelope or specific to NET39. One possible way to address this is by repeating the ChIP experiments in a background of expressing the nucleoplasmic fragment of NET39 fused with a nucleolar localization module, which has been previously shown to recruit the locus towards the nucleolus. If similar deposition of epigenetic marks is observed, this would suggest that this effect is directly dependent on NET39. If not, then it is more likely that NET39 is only involved in recruiting the gene loci to the NE while deposition of epigenetic marks is a general feature of the NE. Alternatively, artificially tethering the locus at the periphery independent of NET39 using CRISPR followed by ChIP will also help in addressing if H3K9Me3 deposition is a general effect of the nuclear periphery. Taken together, our results suggest that a more critical assessment of the 'Interactome' datasets is required. It is possible that the aforementioned partner proteins do regulate features of myogenesis and genome organization but act independent of NET39. The

interactions reflected by our datasets might be a consequence of spatial proximity rather than functional association. Further, effective protein concentrations at the envelope are very high (leading to reduced intermolecular distances) as the volume occupied by transmembrane proteins (which are confined in the 50nm space between INM and ONM) is roughly only 1/30th of the total nuclear volume (Schirmer and De Las Heras, 2014), which might explain why BioID datasets for NE proteins need to be interpreted carefully. The only other NET39 'interactome' study utilized a pulldown approach of myc-tagged NET39 and identified 172 significant interactors, which was significantly lesser than the number of proteins identified by BioID (~500). Unexpectedly, only 22 proteins were shared between both datasets. Further, several of these overlapping proteins appear as insignificant interactors with low spectral abundances in the BioID dataset. It is also possible that interactions identified by BioID might reflect largely transient interactions which are harder to study but biologically significant. Further, the pulldown approach adopted by (Liu et al., 2009) might not have been ideal as several NETs (including NET39) have multiple hydrophobic transmembrane domains which require high salt and detergent conditions combined with extensive sonication for proper solubilization which might disrupt weak interactions and preferentially disrupt nuclear interactions so that ER resident proteins would be more likely to come down as fortuitous partners. Until further breakthrough is made in biochemical approaches to study protein-protein interactions, the current 'Interactome' datasets need to be individually confirmed by alternative methods such as FRET before defining hypotheses centered around these interactions.

Reversibility of Genome Organization

Reversibility in genome organization events have been shown in the studies involving heat shock and osmotic stresses (Amat et al., 2019). Studies involving somatic cell reprogramming have shown that the '4D Nucleome' is partially plastic (Beagan et al., 2016) Our preliminary results suggest that the C2C12 system mirrors some aspects of muscle injury observed in mice. Out of the three genes tested, *Cxcl1* and *Efna5* showed a significant reactivation upon Notexin treatment. However, only *Efna5* repositioned into the nuclear interior upon reactivation, suggesting that release from LADs is not a

necessary condition for transcriptional reactivation. A mechanism involving Notexin mediated depletion of repressive factors might explain our qRT-PCR observations. Further, our preliminary analysis on isolated populations indicate that quiescent MB also show augmented transcription, suggesting that Notexin possibly activates a more general pathway involving myogenic genes. Our FISH results indicate that only *Efna5* locus repositions into the nuclear interior upon Notexin treatment, hinting that a subset of NET39 mediated genome organization changes may occur during mitosis. Consequently, MTs, which are terminally differentiated, may not be able to reverse/modify a subset of genome organization patterns. Previous studies in the past have provided support for this idea (Kumaran and Spector, 2008). A parallel study of NET5 in the lab has shown that NET5 binds specific regions in mitotic chromosomes, suggesting that NET5 establishes LADs patterns during NE reformation (data not shown). In the case of myogenesis, it has been previously suggested that upon induction of differentiation, MBs go through a final division cycle, possibly to facilitate different muscle NETs to establish their specific genome organization patterns.

However, it is also possible that upon reactivation, these genes transit into the A2 genomic compartment to aid repair processes and get recruited back to the nuclear periphery to shutdown post repair. Since the A2 compartment lies within a micron from the NE, it's possible that the sensitivity of 2D FISH analysis is insufficient to capture such a release potentially for *Cxcl1* locus. Other important variables are the durations and concentrations of Notexin treatment itself. These preliminary studies need to be extended to include a much larger concentration range over a larger time scale. We also report a decrease in NET39 transcript levels upon Notexin treatment, hinting at a possible de-differentiation like state. Also, these studies can be made more physiological by performing Notexin treatment on C2C12s co-cultured with functional neurons (Afshar Bakooshli et al., 2019). Further, studies conducted in this system must be extended to live mice by injecting Notexin and following genome organization patterns in different cell types present in the tissue.

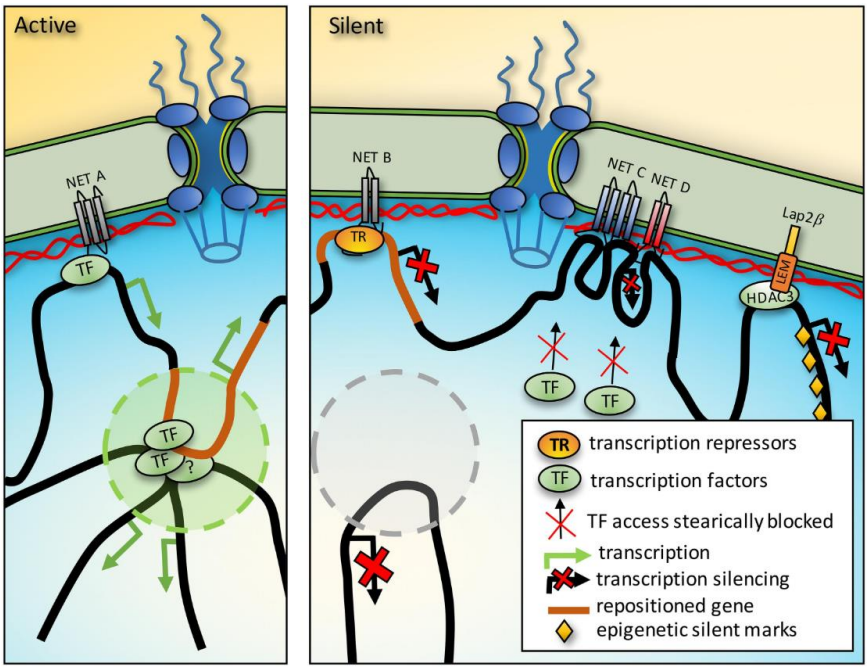

Fig 30) Speculative model of muscle NET mediated genome organization. **Active:** NET interaction with activating TF drives gene expression at periphery. Also, release genes associate with regulatory elements and/or become accessible to nucleoplasmic TFs for upregulation. **Silent:** NET interaction with repressive factors (TR and HDAC3) drives repression at NE. Activating TFs may get sterically excluded from the NE. This is coupled with loss of internal activating A chromatin compartments (Adapted from Czapiewski et al, 2016)

In conclusion, our results (schematically represented in Fig 30) suggest that that myogenic genome organization is associated with massive changes in higher order genome organization and NE-chromatin interactions which facilitate fine-tuning of genes and regulatory elements important for myogenesis. Further, muscle specific NET39 may exploit various interactions with partner proteins, specifically epigenetic modifiers to direct/modulate these changes. Differential interaction profiles with repressive and activating factors may explain why not all LADs are associated with transcriptional repression. Further, tethering of distal sites may also allow internal chromatin compartment assembly, potentially facilitating enhancer-gene associations. Lastly, these genome organization changes occur in a partly reversible manner depending on external cues like pro- differentiation signals or muscle injury.

Bibliography

Afshar Bakooshli, M., Lippmann, E.S., Mulcahy, B., Iyer, N., Nguyen, C.T., Tung, K., Stewart, B.A., van den Dorpel, H., Fuehrmann, T., Shoichet, M., et al. (2019). A 3D culture model of innervated human skeletal muscle enables studies of the adult neuromuscular junction. Elife *8*.

Amat, R., Böttcher, R., Le Dily, F., Vidal, E., Quilez, J., Cuartero, Y., Beato, M., de Nadal, E., and Posas, F. (2019). Rapid reversible changes in compartments and local chromatin organization revealed by hyperosmotic shock. Genome Res. *29*, 18–28.

Amendola, M., and van Steensel, B. (2015). Nuclear lamins are not required for lamina-associated domain organization in mouse embryonic stem cells. EMBO Rep. *16*, 610–617.

Anderson, D.J., and Hetzer, M.W. (2007). Nuclear envelope formation by chromatin-mediated reorganization of the endoplasmic reticulum. Nat. Cell Biol. *9*, 1160–1166.

Batrakou, D.G., de Las Heras, J.I., Czapiewski, R., Mouras, R., and Schirmer, E.C. (2015). TMEM120A and B: nuclear envelope transmembrane proteins important for adipocyte differentiation. PLoS ONE *10*, e0127712.

Beagan, J.A., Gilgenast, T.G., Kim, J., Plona, Z., Norton, H.K., Hu, G., Hsu, S.C., Shields, E.J., Lyu, X., Apostolou, E., et al. (2016). Local Genome Topology Can Exhibit an Incompletely Rewired 3D-Folding State during Somatic Cell Reprogramming. Cell Stem Cell *18*, 611–624.

Beaulieu-Laroche, L., Christin, M., Donoghue, A., Agosti, F., Yousefpour, N., Petitjean, H., Davidova, A., Stanton, C., Khan, U., Dietz, C., et al. (2020). TACAN is an ion channel involved in sensing mechanical pain. Cell *180*, 956-967.e17.

Beyer, S., Pontis, J., Schirwis, E., Battisti, V., Rudolf, A., Le Grand, F., and Ait-Si-Ali, S. (2016). Canonical Wnt signalling regulates nuclear export of Setdb1 during skeletal muscle terminal differentiation. Cell Discov. *2*, 16037.

Bhaskara, R.M., Grumati, P., Garcia-Pardo, J., Kalayil, S., Covarrubias-Pinto, A., Chen, W., Kudryashev, M., Dikic, I., and Hummer, G. (2019). Curvature induction and membrane remodeling by FAM134B reticulon homology domain assist selective ER-phagy. Nat. Commun. *10*, 2370.

Blum, R., Vethantham, V., Bowman, C., Rudnicki, M., and Dynlacht, B.D. (2012). Genome-wide identification of enhancers in skeletal muscle: the role of MyoD1. Genes & Dev. 26: 2763-2779

Bouzid, T., Kim, E., Riehl, B.D., Esfahani, A.M., Rosenbohm, J., Yang, R., Duan, B., and Lim, J.Y. (2019). The LINC complex, mechanotransduction, and mesenchymal stem cell function and fate. J. Biol. Eng. *13*, 68.

Buckle, A., Brackley, C.A., Boyle, S., Marenduzzo, D., and Gilbert, N. (2018). Polymer simulations of heteromorphic chromatin predict the 3D folding of complex genomic loci. Mol. Cell *72*, 786-797.e11.

Caruelle, D., Mazouzi, Z., Husmann, I., Delbé, J., Duchesnay, A., Gautron, J., Martelly, I., and Courty, J. (2004). Upregulation of HARP during in vitro myogenesis and rat soleus muscle regeneration. J. Muscle Res. Cell Motil. *25*, 45–53.

Cremer, M., von Hase, J., Volm, T., Brero, A., Kreth, G., Walter, J., Fischer, C., Solovei, I., Cremer, C., and Cremer, T. (2001). Non-random radial higher-order chromatin arrangements in nuclei of diploid human cells. Chromosome Res. *9*, 541–567.

Criscione, S.W., De Cecco, M., Siranosian, B., Zhang, Y., Kreiling, J.A., Sedivy, J.M., and Neretti, N. (2016). Reorganization of chromosome architecture in replicative cellular senescence. Sci. Adv. *2*, e1500882.

Cull-Candy, S.G., Fohlman, J., Gustavsson, D., Lüllmann-Rauch, R., and Thesleff, S. (1976). The effects of taipoxin and notexin on the function and fine structure of the murine neuromuscular junction. Neuroscience *1*, 175–180.

Demmerle, J., Koch, A.J., and Holaska, J.M. (2012). The nuclear envelope protein emerin binds directly to histone deacetylase 3 (HDAC3) and activates HDAC3 activity. J. Biol. Chem. *287*, 22080–22088.

De Paepe, B., Creus, K.K., Martin, J.-J., and De Bleecker, J.L. (2012). Upregulation of chemokines and their receptors in Duchenne muscular dystrophy: potential for attenuation of myofiber necrosis. Muscle Nerve *46*, 917–925.

Falk, M., Feodorova, Y., Naumova, N., Imakaev, M., Lajoie, B.R., Leonhardt, H., Joffe, B., Dekker, J., Fudenberg, G., Solovei, I., et al. (2019). Heterochromatin drives compartmentalization of inverted and conventional nuclei. Nature *570*, 395–399.

Fan, H., Lv, P., Huo, X., Wu, J., Wang, Q., Cheng, L., Liu, Y., Tang, Q.-Q., Zhang, L., Zhang, F., et al. (2018). The nuclear matrix protein HNRNPU maintains 3D genome architecture globally in mouse hepatocytes. Genome Res. *28*, 192–202.

Ferrai, C., de Castro, I.J., Lavitas, L., Chotalia, M., and Pombo, A. (2010). Gene positioning. Cold Spring Harb. Perspect. Biol. *2*, a000588.

Finlan, L.E., Sproul, D., Thomson, I., Boyle, S., Kerr, E., Perry, P., Ylstra, B., Chubb, J.R., and Bickmore, W.A. (2008). Recruitment to the nuclear periphery can alter expression of genes in human cells. PLoS Genet. *4*, e1000039.

Frost, B., Bardai, F.H., and Feany, M.B. (2016). Lamin dysfunction mediates neurodegeneration in tauopathies. Curr. Biol. *26*, 129–136.

Furukawa, K., Sugiyama, S., Osouda, S., Goto, H., Inagaki, M., Horigome, T., Omata, S., McConnell, M., Fisher, P.A., and Nishida, Y. (2003). Barrier-to-autointegration factor

plays crucial roles in cell cycle progression and nuclear organization in Drosophila. J. Cell Sci. *116*, 3811–3823.

Greenwald, W.W., Chiou, J., Yan, J., Qiu, Y., Dai, N., Wang, A., Nariai, N., Aylward, A., Han, J.Y., Kadakia, N., et al. (2019). Pancreatic islet chromatin accessibility and conformation reveals distal enhancer networks of type 2 diabetes risk. Nat. Commun. *10*, 2078.

Greil, F., Moorman, C., and van Steensel, B. (2006). DamID: mapping of in vivo protein-genome interactions using tethered DNA adenine methyltransferase. Meth. Enzymol. *410*, 342–359.

Guelen, L., Pagie, L., Brasset, E., Meuleman, W., Faza, M.B., Talhout, W., Eussen, B.H., de Klein, A., Wessels, L., de Laat, W., et al. (2008). Domain organization of human chromosomes revealed by mapping of nuclear lamina interactions. Nature *453*, 948–951.

Gurtner, A., Fuschi, P., Magi, F., Colussi, C., Gaetano, C., Dobbelstein, M., Sacchi, A., and Piaggio, G. (2008). NF-Y dependent epigenetic modifications discriminate between proliferating and postmitotic tissue. PLoS ONE *3*, e2047.

Happe, C.L., and Engler, A.J. (2016). Mechanical forces reshape differentiation cues that guide cardiomyogenesis. Circ. Res. *118*, 296–310.

Hetzer, M.W. (2010). The nuclear envelope. Cold Spring Harb. Perspect. Biol. *2*, a000539.

Korfali, N., Wilkie, G.S., Swanson, S.K., Srsen, V., Batrakou, D.G., Fairley, E.A.L., Malik, P., Zuleger, N., Goncharevich, A., de Las Heras, J., et al. (2010). The leukocyte nuclear envelope proteome varies with cell activation and contains novel transmembrane proteins that affect genome architecture. Mol. Cell. Proteomics *9*, 2571–2585.

Korfali, N., Wilkie, G.S., Swanson, S.K., Srsen, V., de Las Heras, J., Batrakou, D.G., Malik, P., Zuleger, N., Kerr, A.R.W., Florens, L., et al. (2012). The nuclear envelope proteome differs notably between tissues. Nucleus *3*, 552–564.

Kukalev, A.S., Lobov, I.B., Percipalle, P., and Podgornaya, O.I. (2009). SAF-A/hnRNP-U localization in interphase and metaphase. Cytogenet. Genome Res. *124*, 288–297.

Kumaran, R.I., and Spector, D.L. (2008). A genetic locus targeted to the nuclear periphery in living cells maintains its transcriptional competence. J. Cell Biol. *180*, 51–65.

Kumaran, R.I., Thakar, R., and Spector, D.L. (2008). Chromatin dynamics and gene positioning. Cell *132*, 929–934.

Labade, A.S., Karmodiya, K., and Sengupta, K. (2016). HOXA repression is mediated

by nucleoporin Nup93 assisted by its interactors Nup188 and Nup205. Epigenetics Chromatin *9*, 54.

de Las Heras, J.I., Zuleger, N., Batrakou, D.G., Czapiewski, R., Kerr, A.R.W., and Schirmer, E.C. (2017). Tissue-specific NETs alter genome organization and regulation even in a heterologous system. Nucleus *8*, 81–97.

Lieberman-Aiden, E., van Berkum, N.L., Williams, L., Imakaev, M., Ragoczy, T., Telling, A., Amit, I., Lajoie, B.R., Sabo, P.J., Dorschner, M.O., et al. (2009). Comprehensive mapping of long-range interactions reveals folding principles of the human genome. Science *326*, 289–293.

Liu, G.-H., Guan, T., Datta, K., Coppinger, J., Yates, J., and Gerace, L. (2009). Regulation of myoblast differentiation by the nuclear envelope protein NET39. Mol. Cell. Biol. *29*, 5800–5812.

Li, G., Liu, Y., Zhang, Y., Kubo, N., Yu, M., Fang, R., Kellis, M., and Ren, B. (2019). Joint profiling of DNA methylation and chromatin architecture in single cells. Nat. Methods *16*, 991–993.

Lupiáñez, D.G., Kraft, K., Heinrich, V., Krawitz, P., Brancati, F., Klopocki, E., Horn, D., Kayserili, H., Opitz, J.M., Laxova, R., et al. (2015). Disruptions of topological chromatin domains cause pathogenic rewiring of gene-enhancer interactions. Cell *161*, 1012–1025.

Lyu, H., Liu, E., and Wu, Z. (2020). Comparison of normalization methods for Hi-C data. BioTechniques *68*, 56–64.

Mas, G., Blanco, E., Ballaré, C., Sansó, M., Spill, Y.G., Hu, D., Aoi, Y., Le Dily, F., Shilatifard, A., Marti-Renom, M.A., et al. (2018). Promoter bivalency favors an open chromatin architecture in embryonic stem cells. Nat. Genet. *50*, 1452–1462.

Mehta, I.S., Amira, M., Harvey, A.J., and Bridger, J.M. (2010). Rapid chromosome territory relocation by nuclear motor activity in response to serum removal in primary human fibroblasts. Genome Biol. *11*, R5.

Meinke, P., Mattioli, E., Haque, F., Antoku, S., Columbaro, M., Straatman, K.R., Worman, H.J., Gundersen, G.G., Lattanzi, G., Wehnert, M., et al. (2014). Muscular dystrophy-associated SUN1 and SUN2 variants disrupt nuclear-cytoskeletal connections and myonuclear organization. PLoS Genet. *10*, e1004605.

Meinke, P., Kerr, A.R.W., Czapiewski, R., de Las Heras, J.I., Dixon, C.R., Harris, E., Kölbel, H., Muntoni, F., Schara, U., Straub, V., et al. (2020). A multistage sequencing strategy pinpoints novel candidate alleles for Emery-Dreifuss muscular dystrophy and supports gene misregulation as its pathomechanism. EBioMedicine *51*, 102587.

Nagano, T., Lubling, Y., Stevens, T.J., Schoenfelder, S., Yaffe, E., Dean, W., Laue,

E.D., Tanay, A., and Fraser, P. (2013). Single-cell Hi-C reveals cell-to-cell variability in chromosome structure. Nature *502*, 59–64.

Ou, H.D., Phan, S., Deerinck, T.J., Thor, A., Ellisman, M.H., and O'Shea, C.C. (2017). ChromEMT: Visualizing 3D chromatin structure and compaction in interphase and mitotic cells. Science *357*.

O'Shaughnessy-Kirwan, A., Signolet, J., Costello, I., Gharbi, S., and Hendrich, B. (2015). Constraint of gene expression by the chromatin remodelling protein CHD4 facilitates lineage specification. Development *142*, 2586–2597.

Peric-Hupkes, D., and van Steensel, B. (2010). Role of the nuclear lamina in genome organization and gene expression. Cold Spring Harb. Symp. Quant. Biol. *75*, 517–524.

Pradhan, R., Ranade, D., and Sengupta, K. (2018). Emerin modulates spatial organization of chromosome territories in cells on softer matrices. Nucleic Acids Res. *46*, 5561–5586.

Pradhan, R., Nallappa, M.J., and Sengupta, K. (2020). Lamin A/C modulates spatial organization and function of the Hsp70 gene locus via nuclear myosin I. J. Cell Sci. *133*.

Prokocimer, M., Davidovich, M., Nissim-Rafinia, M., Wiesel-Motiuk, N., Bar, D.Z., Barkan, R., Meshorer, E., and Gruenbaum, Y. (2009). Nuclear lamins: key regulators of nuclear structure and activities. J. Cell. Mol. Med. *13*, 1059–1085.

Rao, S.S.P., Huntley, M.H., Durand, N.C., Stamenova, E.K., Bochkov, I.D., Robinson, J.T., Sanborn, A.L., Machol, I., Omer, A.D., Lander, E.S., et al. (2014). A 3D map of the human genome at kilobase resolution reveals principles of chromatin looping. Cell *159*, 1665–1680.

Robertson, K.D., Ait-Si-Ali, S., Yokochi, T., Wade, P.A., Jones, P.L., and Wolffe, A.P. (2000). DNMT1 forms a complex with Rb, E2F1 and HDAC1 and represses transcription from E2F-responsive promoters. Nat. Genet. *25*, 338–342.

Robson, M.I., de Las Heras, J.I., Czapiewski, R., Lê Thành, P., Booth, D.G., Kelly, D.A., Webb, S., Kerr, A.R.W., and Schirmer, E.C. (2016). Tissue-Specific Gene Repositioning by Muscle Nuclear Membrane Proteins Enhances Repression of Critical Developmental Genes during Myogenesis. Mol. Cell *62*, 834–847.

Robson, M.I., de Las Heras, J.I., Czapiewski, R., Sivakumar, A., Kerr, A.R.W., and Schirmer, E.C. (2017). Constrained release of lamina-associated enhancers and genes from the nuclear envelope during T-cell activation facilitates their association in chromosome compartments. Genome Res. *27*, 1126–1138.

Schirmer, E.C., Florens, L., Guan, T., Yates, J.R., and Gerace, L. (2003). Nuclear membrane proteins with potential disease links found by subtractive proteomics. Science *301*, 1380–1382.

Stark, D.A., Karvas, R.M., Siegel, A.L., and Cornelison, D.D.W. (2011). Eph/ephrin interactions modulate muscle satellite cell motility and patterning. Development *138*, 5279–5289.

Taniura, H., Glass, C., and Gerace, L. (1995). A chromatin binding site in the tail domain of nuclear lamins that interacts with core histones. J. Cell Biol. *131*, 33–44.

Thomou, T., Mori, M.A., Dreyfuss, J.M., Konishi, M., Sakaguchi, M., Wolfrum, C., Rao, T.N., Winnay, J.N., Garcia-Martin, R., Grinspoon, S.K., et al. (2017). Adipose-derived circulating miRNAs regulate gene expression in other tissues. Nature *542*, 450–455.

Towbin, B.D., Gonzalez-Sandoval, A., and Gasser, S.M. (2013). Mechanisms of heterochromatin subnuclear localization. Trends Biochem. Sci. *38*, 356–363.

Wang, J., Li, X., Wang, L., Li, J., Zhao, Y., Bou, G., Li, Y., Jiao, G., Shen, X., Wei, R., et al. (2016a). A novel long intergenic noncoding RNA indispensable for the cleavage of mouse two-cell embryos. EMBO Rep. *17*, 1452–1470.

Wang, S., Tukachinsky, H., Romano, F.B., and Rapoport, T.A. (2016b). Cooperation of the ER-shaping proteins atlastin, lunapark, and reticulons to generate a tubular membrane network. Elife *5*.

Wijchers, P.J., Geeven, G., Eyres, M., Bergsma, A.J., Janssen, M., Verstegen, M., Zhu, Y., Schell, Y., Vermeulen, C., de Wit, E., et al. (2015). Characterization and dynamics of pericentromere-associated domains in mice. Genome Res. *25*, 958–969.

Worman, H.J., and Schirmer, E.C. (2015). Nuclear membrane diversity: underlying tissue-specific pathologies in disease? Curr. Opin. Cell Biol. *34*, 101–112.

Xu, J., Ma, H., Jin, J., Uttam, S., Fu, R., Huang, Y., and Liu, Y. (2018). Super-Resolution Imaging of Higher-Order Chromatin Structures at Different Epigenomic States in Single Mammalian Cells. Cell Rep. *24*, 873–882.

Ye, Q., and Worman, H.J. (1996). Interaction between an integral protein of the nuclear envelope inner membrane and human chromodomain proteins homologous to Drosophila HP1. J. Biol. Chem. *271*, 14653–14656.

Yejing Ge et al (2011). MicroRNAs in skeletal myogenesis, Cell Cycle. 10:3, *441-448*

Zuleger, N., Boyle, S., Kelly, D.A., de las Heras, J.I., Lazou, V., Korfali, N., Batrakou, D.G., Randles, K.N., Morris, G.E., Harrison, D.J., et al. (2013). Specific nuclear envelope transmembrane proteins can promote the location of chromosomes to and from the nuclear periphery. Genome Biol. *14*, R14.

Zullo, J.M., Demarco, I.A., Piqué-Regi, R., Gaffney, D.J., Epstein, C.B., Spooner, C.J., Luperchio, T.R., Bernstein, B.E., Pritchard, J.K., Reddy, K.L., et al. (2012). DNA sequence-dependent compartmentalization and silencing of chromatin at the nuclear lamina. Cell *149*, 1474–1487.